Multifunctional Graphene and Carbon Nanotube films for Planar Heterojunction Solar Cells

Kehang Cui[1] and Shigeo Maruyama[2,3]

[1] Department of Mechanical Engineering, Massachusetts Institute of Technology, Cambridge, MA 02139, USA
Email: cuik@mit.edu

[2] Department of Mechanical Engineering, The University of Tokyo, Tokyo 113-8656, Japan
E-mail: maruyama@photon.t.u-tokyo.ac.jp

[3] Energy NanoEngineering Laboratory, National Institute of Advanced Industrial Science and Technology (AIST), Tsukuba 305-8564, Japan

Abstract

Graphene and carbon nanotubes, featured with outstanding electronic, photonic and mechanical properties as well as Earth abundancy, are perfect for use as carrier-selective transport and collecting layers in photovoltaics. In recent years, graphene and carbon nanotube films have underpinned significant advancement in the planar heterojunction (PHJ) solar cells with Si/GaAs as photoactive materials. With reduced fabrication cost and improved power conversion efficiencies approaching 20%, graphene-based and carbon nanotube-based PHJ solar cells possess great potential for scalable deployment. We summarize the state-of-art progress in graphene-based and carbon nanotube-based PHJ solar cells leveraging advanced nanocarbon technologies as well as industrial-compatible solar cell design and processing. Tuning of Fermi level, electrical and photonic properties of graphene and carbon nanotube films for PHJ solar cells are systematically reviewed. We also envision technological pathways and future prospects to exploit multifunctionality of graphene and carbon nanotubes to realize ubiquitous application of high-performance, flexible PHJ solar cells.

1. Introduction

Solar cells can directly convert solar energy to electric power without carbon footprint, and thus are promising to meet world energy consumption demands and fulfil low carbon scenario in future. A typical planar heterojunction (PHJ) solar cell has three main components: a top electrode layer (or emitter) to create built-in potential for separating electron-hole pairs and selectively transporting electrons/holes, a photoactive layer to absorb solar energy and generate electron-hole pairs, as well as a bottom electrode layer (or base) to collect holes/electrons. Compared with p-n junction solar cells, PHJ solar cells have a simpler structure and do not require high-temperature dopant diffusion processes, which allows compatible and scalable manufacturing and cuts fabrication cost up to 30% [1-3].

In a PHJ solar cell, the top electrode layer is required to have high electrical conductivity and optical transparency simultaneously, with appropriate electronic band structure and Fermi level position matching the used photoactive layer. These requirements are usually realized by a double-layer design comprising of a transparent conductive film (TCF) and a selective hole/electron transport layer. The conventional materials for TCFs are noble metal grids (such as silver and gold) and degenerately doped metal oxides (such as indium-doped tin oxide (ITO)). However, the elemental scarcity and high cost of the noble metals and indium-doped oxides potentially prevent their use at scale. For the selective hole/electron transport layer, the commonly used materials are conductive organic materials such as poly(3,4-ethylenedioxythiophene):poly(styrene sulfonate) (PEDOT:PSS) and lithium bis(trifluoromethylsulphonyl)imide-doped 2,2′,7,7′-tetrakis(N,N-di-p-methoxyphenylamine)-9,9′-spirobifluorene (spiro-OMeTAD:LiTFSI). PEDOT:PSS and spiro-OMeTAD:LiTFSI are inhomogeneous dispersions which suffer from instability and degradation of electrical

conductivity [4]. Additionally, PEDOT:PSS is highly acidic (pH~1) which may corrode ITO and other components in PHJ solar cells. Therefore, it is highly desirable to develop new materials for the top electrode layers of the PHJ solar cells.

Graphene and single-walled carbon nanotubes (SWNTs) are atomic-thin sp2 hybridized carbon materials. The strong covalent π bonds in graphene and SWNTs enable ballistic electronic and thermal transport, excellent mechanical strength and flexibility, as well as good chemical inertness and stability. Moreover, graphene and SWNTs are Earth-abundant materials which can be synthesized by scalable chemical vapor deposition (CVD) process. Compared with metals, ITO and conductive polymers, graphene and SWNTs have several advantages as top electrode materials for PHJ solar cells. First, the Fermi levels of graphene and SWNTs can be easily tuned because of their low electronic density of states. Through appropriate functionalization, higher built-in potential to separate electron-hole pairs can be realized at the junction between nanocarbon electrode and photoactive layer. Second, graphene and SWNTs have higher electrical conductivity and optical transparency, which allows more efficient charge separation and collection at the junction to achieve higher power conversion efficiencies (PCEs). Third, graphene and SWNTs are low-dimensional materials, thus they can be assembled into various morphologies and hierarchical structures, providing flexibility in structural design of nanocarbon-based PHJ solar cells. In addition, graphene and SWNTs films can be transferred onto arbitrary substrates at room temperature, which can decouple preparation and deposition of high-performance top electrodes. This would result in a better junction quality and allow more flexible and scalable fabrication of PHJ solar cells.

For the photoactive layer of a PHJ solar cell, inorganic semiconductor materials, such as Si and GaAs, have superiorities over lead halide perovskite [5-7] and polymers [8] in terms of long-

term durability, low toxicity, abundant raw material supply and scalable fabrication technologies for cells and modules. Moreover, Si and GaAs have been through decades of perfection in material quality and maturation in production line [9]. Combining the technological know-hows of Si and GaAs with graphene-based and SWNT-based transparent top electrodes holds the promise to further improve PCE and decrease fabrication cost, thereby paving the way of realizing scale-up deployment of photovoltaics as a renewable source of electricity.

PHJ solar cells comprised of multifunctional nanocarbon electrodes and inorganic semiconductor materials have drawn widespread attention, with PCEs rocketing to 14 – 17% within few years [10-13]. The disruptive development is mainly benefitted from the accumulated knowledge of nanocarbon technologies and solar cell mechanisms. Extensive efforts have been focused on chemical functionalization, device structural design as well as light management of the nanocarbon-based PHJ solar cells. This review focuses on advanced functionalization strategies for improving device performance of graphene-based and CNT-based PHJ solar cells as well as discusses their fundamental mechanisms. The chemical functionalization for tuning Fermi level, which is the cornerstone for high device performance, is discussed first. Molecular adsorption (gas-phase doping), electrochemical gating (liquid-phase doping) and solid-state functionalization (solid-phase doping) are evaluated based on their effectiveness and stability. Then morphological design and hybrid structures of graphene and CNTs to achieve higher electrical conductivity and optical transparency are reviewed. The structural design also focuses on the interface between nanocarbon films and photoactive materials which is critical to the charge separation and collection. In addition, photonic design is discussed including light trapping of PHJ solar cells and plasmonic-induce field enhancement. In the last section, the recent progress in flexible graphene-based and SWNT-based PHJ solar cells are also reviewed.

2. State of the art of PHJ solar cells

2.1 Evaluation of Photoactive Materials

Currently the most commercially competitive photoactive materials for PHJ solar cells include crystalline silicon (c-Si), cadmium telluride (CdTe) and copper indium gallium selenide (CIGS). With 75 GW installation in 2016, c-Si is dominating the solar-cell market, taking up to 93% of market share [14]. CdTe and CIGS utilize less photoactive semiconductor material per watt than c-Si, however, both are very expensive and contain rare-earth materials, and can be toxic to human beings. Recently, the PCE of lead halide perovskite solar cells (PSCs) has increased from 3.8% [15] to 22.1% [16] since its first embodiment in 2009. As the PCE values of PSCs approaching those of commercially available solar cells, evaluations of their potential in market is on the agenda. Although the PCE is the most sought-after and eye-catching property of a solar cell in laboratory, stability of PCE, scalability, manufacturing cost, elemental scarcity, toxicity are equally important factors for practical applications and massive deployment.

Scalability. The surge in performance of PSCs is mostly based on small-area devices (0.1 cm^2) in laboratory, owing to the improved composition and morphology of perovskite thin films through solution chemistry and interface optimization. However, the efficiencies of PSC modules dropped drastically to 12.1% [17, 18] when device area increased to 16 cm^2, whereas the PCE of c-Si only changed from 26.7% to 24.5% [9] when device area increased from 79 cm^2 to 13177 cm^2. The PCE of PSCs degrades much faster with the increase of device area owing to the non-uniformity of the film.

Stability. The stability of the PCE is of equal importance to the absolute value of PCE, both of which determine the electricity generated by the solar cell system over its operational lifetime.

Inorganic solar cells, such as c-Si, CdTe and CIGS, have an operational lifetime of over 25 years. Metal halide perovskite (ABX$_3$) has intrinsically and extrinsically low structural stability owing to the weak interactions of the A cation with B and X, as well as the interaction between layers, thus the PCEs of PSCs are prone to decay when exposed to humidity, heat, light, oxygen, *etc*. Both scalability and stability limit the practical applications of PSCs, which may not be solved in a short term.

Environment, health and safety (EHS). Silicon is one of the most abundant element on earth and non-toxic, which makes it perfect for massive deployment. An important disadvantage of perovskite materials in their current form is that they contain heavy metals, such as lead. Potential EHS issues exist in all the five stages of a PSC life cycle: (1) raw material extraction, (2) synthesis of starting products, (3) fabrication, (4) use and (5) decommissioning [19]. Especially, the overall burden of organolead compounds is considered much higher than their inorganic counterparts, as they can readily pass biological barriers to reach vital areas due to their relatively high fat solubility. Advanced encapsulation on a module level is required for PSCs, which causes extra cost. Moreover, the current high-performance PSCs require electrodes using rare-earth metals which is not environmentally friendly.

Manufacturing Cost. Perovskite materials have low formation energies for deposition and are compatible with scalable manufacturing techniques such as roll-to-roll printing. Thus they have the potential of low production costs and capital expenditure. However, the fabrication of high-performance PSCs (with PCE of *ca.* 20%) usually requires expensive materials, fine control of morphology for each layer, and a vacuum deposition process, which has very high cost. On the other hand, PSCs with full printable structures realized by low-cost materials and processes have PCEs below 15% [20-22]. The photoactive semiconductor material accounts for about 60% of c-

Si module cost [2]. The cost of polysilicon for c-Si modules could be reduced by making thinner wafers, minimizing polysilicon losses during the wafering process, improving polysilicon scrap recycling capabilities and costs, and introducing low-cost polysilicon feedstock-purification methods.

As stated above, to compete with c-Si in the PV market, the PCE and lifetime of PSCs are required to be beyond 15% and 15 years, respectively, with heavy metals in the perovskite materials replaced. This means magnificent amount of investment in laboratory-scale research as well as years of learning curve in industry-scale installation and deployment. It is more reasonable to integrate emerging materials with sophisticated c-Si and other thin-film PV technologies to realize high-efficiency and low-cost solar cells.

2.2 Graphene and Carbon Nanotube Films for PHJ PV

The prototype nanocarbon/Si PHJ solar cell is constructed by a moderately doped Si photoactive layer sandwiched by thin graphene or carbon nanotube film as emitter and rear metal electrode. The valence-band electrons in the photoactive semiconductor material, *i.e.* Si or GaAs, are excited by absorbing photons with energy greater than the bandgap energy, generating electron-hole pairs, which are then separated by the electric field at the nanocarbon/semiconductor junction. The holes (electrons) are then collected by the nanocarbon layer for *p*-nanocarbon/*n*-semiconductor (*n*-nanocarbon/*p*-semiconductor) junction once they drift to the junction. The circuit is complete once the holes (electrons) pass through the load and meet up the electrons (holes) in the *n*-semiconductor (*p*-semiconductor). Unlike metals, the Fermi level of the nanocarbon layer could be shifted through doping, even for metallic SWNTs and graphene which behaves metallic. Therefore, the quantum nature of the nanocarbons determines that the nanocarbon-semiconductor junction is a heterojunction rather than a Schottky junction. The strongest advantage of a heterojunction over a

7

homojunction is the minimized charge carrier recombination loss at the surfaces of Si wafer, which is embodied by recent record efficiencies of 25.1% and 26.3% for c-Si PHJ solar cells.

The nanocarbon layer in a PHJ solar cell serves as both the transparent conductive layer and the hole collecting layer. Heavily doped nanocarbon layer also serves to create depletion layer to tunnel the charge carriers through the passivation layer. This would not only simplify the structure significantly, but also enable decoupled fabrication and transfer deposition of all the top layers. Moreover, nanocarbon materials could avoid the usage of rare-earth metals which is vital in transparent conductive oxide, and reduce the manufacturing cost of plasmon-enhanced CVD and sputtering required in clean-room setup. Another distinctive feature of nanocarbon materials is their exceptional tunability. Chirality, layer, length, alignment, thickness and doping level are all tuning factors, which can be optimized separately. The nanocarbon layer can be transferred onto the semiconductor substrate through roll-to-roll printing deposition.

3. Fermi Level Tuning

3.1 Fundamentals of Graphene and Carbon Nanotubes

Graphene and SWNTs are sp2 hybridized nanocarbon materials. In graphene, the wavefunction overlapping of the conjugate π bonds in the hexagon of carbon atoms results in the delocalized π and π * bands, *i.e.* the conduction band (CB) and valence band (VB). The cone-shaped CB and VB intersect at the Dirac point where the Fermi level crosses, making the electrons massless Dirac fermions (Figure 1a). This unique electronic feature leads to a high electron mobility ($\sim 2 \times 10^5$ cm^2 V^{-1} s^{-1} at room temperature [23]) in graphene. Rolling graphene into SWNTs generates curvature-induced quantum confinement. The CB and VB of SWNTs become discontinuous cutting lines on the cone-shaped CB and VB of graphene. Each cutting line gives one π- π* band. If the cutting lines happen to come across the Dirac

point, the SWNT is metallic (Figure 1b); if not, the SWNT is semiconducting (Figure 1c) with bandgaps up to 2 eV. SWNTs inherit the high electron mobility of graphene.

The electronic density of states is extremely low near the Fermi levels of both graphene and SWNTs. The free carrier concentration is $\sim 10^{20}$ cm^{-3} for pristine graphene (or $\sim 10^{12}$ cm^{-2} for planar distribution), and is $\sim 10^{17}$ cm^{-3} for SWNTs, both of which are orders of magnitude lower than that of bulk metals. Chemical functionalization could effectively shift the Fermi levels of graphene and SWNTs. The high tunability of Fermi level in graphene [24] and SWNTs [25] can be demonstrated by continuous band filling through electrochemical gating. As shown in the waterfall Raman spectra in Figure 1d, the remarkable shift of G and G′ band positions of graphene was realized at relatively low gate voltages [24]. The similar phenomenon was also observed in SWNTs [25]. Fermi level tuning could increase the charge carrier density in graphene and SWNTs to realize higher electrical conductivity. Moreover, chemical functionalization could eliminate the Schottky barrier between the metallic and semiconducting SWNTs, and thus could further improve the electrical conductivity of SWNTs. In the sp2 hybridized nanocarbon family, graphite and multiwall CNTs (MWNTs) are multi-layer allotropes of graphene and SWNTs. Graphite and MWNTs have much higher inherent carrier density and hence are more challenging to be doped, yet they have much lower production cost. This chapter reviews chemical functionalization of nanocarbon materials through molecular absorption, electrochemical gating and solid-state functionalization. For practical applications, the stability and Fermi level tunability are the most important criteria for evaluating chemical functionalization effect.
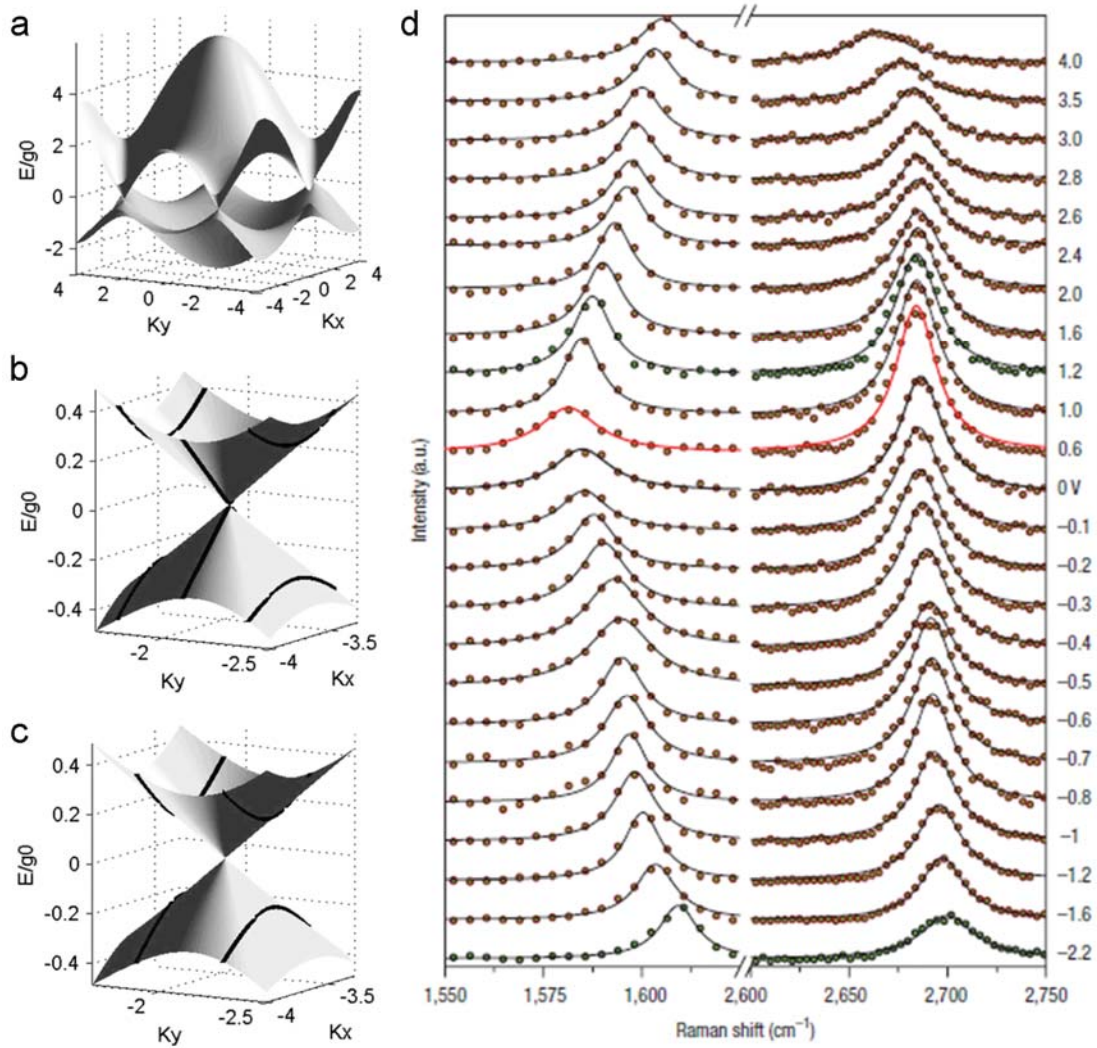
Figure 1. Electronic density of states of (a) graphene, (b) metallic SWNT and (c) semiconducting SWNT. (d) Raman spectra of continuous band filling of graphene by electrochemical gating. Reproduced with permission from Ref. [24]. Copyright 2008, Nature Publishing Group.

3.2 Molecular Adsorption

The high aspect ratio and large surface area of graphene and SWNTs are especially beneficial for molecular adsorption. The charge-transfer process occurs immediately after the direct exposure of a graphene or SWNT film to the functionalizing molecules in gas or solution phase. The functionalization

process could be either p-type or n-type, which is respectively induced by electron acceptor or donor. The doping effectiveness and stability at room temperature are of equal importance.

Strong oxidizing molecules, such as HNO_3 [26-28], H_2SO_4 [29], $SOCl_2$ [30], $AuCl_3$ ($HAuCl_4$) [31-33] and O_3 [34-36] have been extensively investigated as effective p-type dopants for graphene and SWNTs. Specifically, the infiltration of HNO_3 aqueous solution into the CNT film (mixture of MWNTs and SWNTs) in the CNT/Si PHJ solar cell improved the open-circuit voltage (V_{oc}), short-circuit current (J_{sc}) and fill factor (FF) simultaneously, leading to a two-fold PCE increase from 7% to 13.8% [37]. The HNO_3 doping reduced the sheet resistance of the CNT film and significantly decreased the series resistance of the CNT/Si PHJ solar cell on the device level [38-40]. The HNO_3 doping also shifted the Fermi level of CNTs downwards, resulting in the increased built-in potential and V_{oc} of the CNT/Si PHJ solar cell. However, the HNO_3 doping is relatively instable. The PCE of the HNO_3-doped CNT/Si PHJ solar cell decreased from 13.8% to 8.4% after 24 hr storage in the ambient [37]. In fact, the main drawback of the molecular-adsorption functionalization is the instability in the ambient, which may degrade the PCEs of the PHJ solar cells up to 50% in days. The effectiveness and stability of four representative p-type doping molecules (HNO_3, $SOCl_2$, H_2O_2 and HCl) were compared in Figure 2a, based on their functionalization performance in the graphene/Si PHJ solar cells [41]. All the four p-type dopants significantly increased the PCEs of the graphene/Si PHJ solar cells by more than 200%. Among the four molecules, $SOCl_2$ was the most effective dopant which improved the PCE of the graphene/Si PHJ solar cell by 230%. After 8 days storage in the ambient, $SOCl_2$ and HCl showed slightly better doping stability than HNO_3 and H_2O_2, which may be resulted from the more persistent adsorption of Cl atoms serving as the inter-tube linker [42]. Fluorine-based doping agent bis(trifluoromethanesulfonyl)-amide (($CF_3SO_2)_2NH$) (TFSA) was also applied to the graphene/Si PHJ solar cell, which improved the PCE from 1.9% to 8.6%. After 3 days storage in the ambient, the PCE only degraded by 10% [43].

Therefore, halogen-containing molecules are regarded as promising p-type dopants for graphene-based and SWNT-based PHJ solar cells because of their high doping efficacy and stability.

Combination of two or more electron extracting molecules could further enhance p-type doping effect. Jung et al [44] reported a doping method which combined chlorosulfonic acid and gold chloride ($AuCl_3$), both of which were strong p-type dopants to SWNTs [45]. A PCE of 11% was achieved after doping for the SWNT/Si PHJ solar cell in the dry state. By measuring *J-V* characteristics under different operating temperatures, the activation energy (built-in potential) of the SWNT/Si PHJ solar cell was extracted as 1.56 eV using the Schottky-Mott standard model. This value was higher than those of the conventional metal-semiconductor (M-S) and metal-insulator-semiconductor Schottky solar cells. The heavily p-doped SWNT film could induce a p-type inversion layer onto the surface of the n-type Si, resulting in an equivalent p-n junction at room temperature. This ambient doping method could save fabrication cost up to 35%, compared with the conventional high-temperature diffusion processes for generating p-n junctions [46-48]. The stability of the p-type doping could be further improved by sealing solar cells with polydimethylsiloxane (PDMS) [49].

Unlike p-type doping, n-type doping of graphene and SWNTs is difficult to be realized in the ambient, because the oxygen adsorption in the ambient could p-dope graphene and SWNTs and neutralize the n-type doping effect. Typical electron-donors such as alkali metals [50-52] could achieve n-type doping of graphene and SWNTs. However, alkali metals such as K and Rb are instable in the ambient and thus not suitable for practical applications in solar cells. Li et al [53] realized n-type doping of the SWNT/Si PHJ solar cells using metallocene [54-56]. After evacuating in high vacuum for 48 hr, the electron-rich metallocene – Cp_2Co and Cp_2Ni, as well as the closely related complex bis(benzene)chromium (($C_6H_6)_2Cr$) were spin coated onto the SWNT/p-Si PHJ solar cells at room temperature. The molecular structures of the three organometallic compounds are given in Figure 2b.

Compared with the chemically stable ferrocene (18 valence electrons), Cp_2Co and Cp_2Ni have 19 and 20 valence electrons respectively, and thus are ready to donate the extra electrons. The PCE of the Cp_2Co-doped SWNT/p-Si PHJ solar cell was 3.82%, which was 450 times higher than the previously reported pristine SWNT/p-Si PHJ solar cells [57]. The molecular orbital energies of Cp_2Co, $(C_6H_6)_2Cr$ and Cp_2Ni were calculated by density functional theory (DFT) simulation to investigate the doping mechanism. Figure 2c shows the highest occupied molecular orbitals (HOMO) levels of the three organometallic compounds, using hydrazine [58] as a reference. Cp_2Co was found to have the highest HOMO level and the highest tendency to donate electrons to SWNTs. The *J-V* characteristics of the n-SWNT/p-Si PHJ solar cells in Figure 2d demonstrate that the dopant HOMO level is positively correlated to the sheet resistance reduction of the SWNT film as well as the performance improvement of the n-SWNT/p-Si PHJ solar cell. In addition, the Cp2Co-doped SWNT/p-Si PHJ solar cells were more stable than the hydrazine-doped ones [53]. Nitrogen-containing molecules, such as tetracyano-p-quinodimethane (TCNQ) [59, 60], triphenylmethane carbinol base (TPM-CB) [61] and polyethyleneimine (PEI) [62, 63], have been reported as effective n-type dopants for graphene and SWNTs. However, these molecules have not been applied to graphene-based and SWNT-based PHJ solar cells yet.
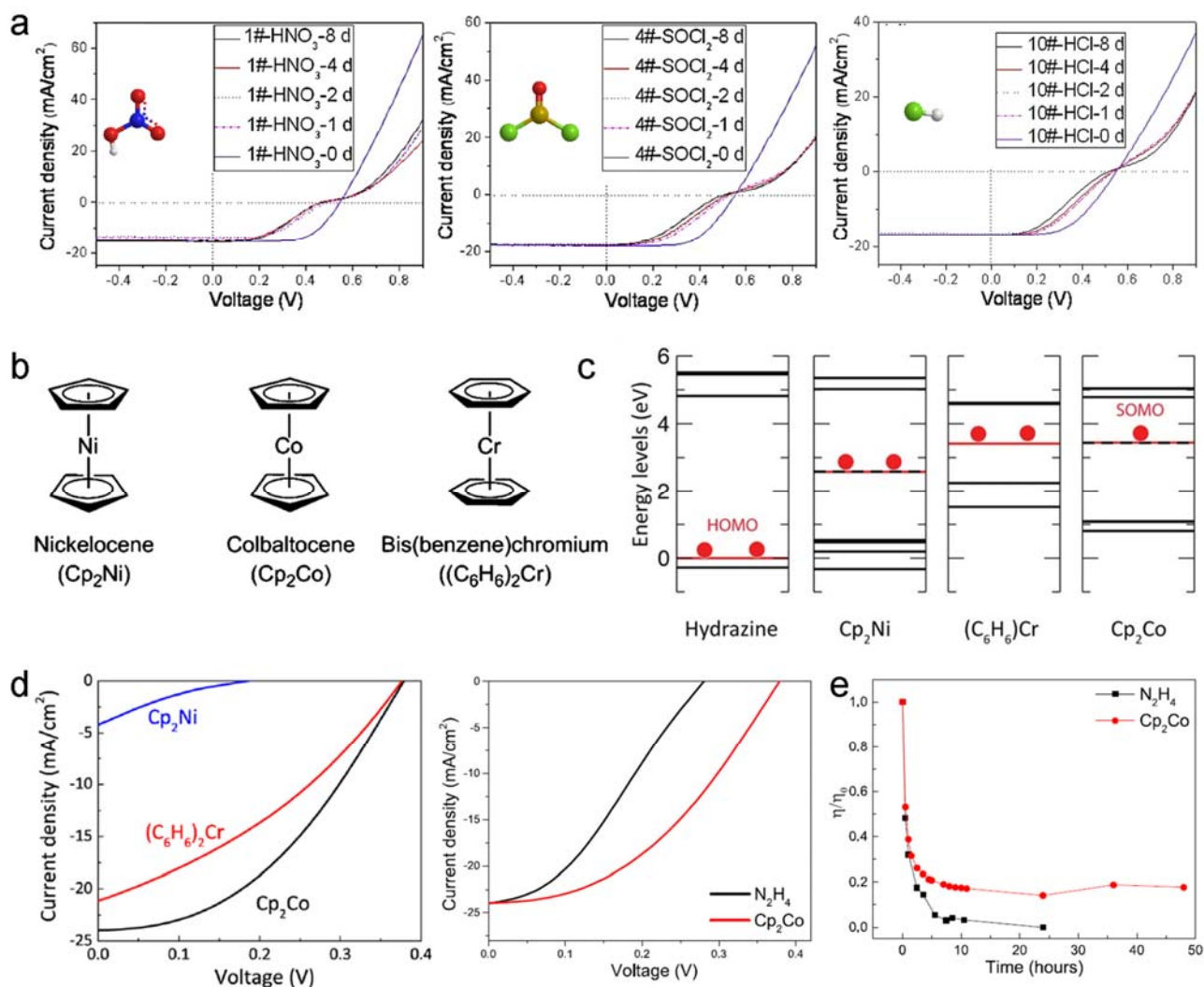
Figure 2. (a) Comparison of different p-type dopants on the *J-V* characteristics of the graphene/Si PHJ solar cells before and after volatile oxidant treatment. Reproduced with permission from Ref. [41]. Copyright 2013, Royal Society of Chemistry. (b) Molecular structures of Cp_2Ni, Cp_2Co and $(C_6H_6)_2Cr$. (c) Calculated highest occupied molecular orbitals (HOMO) levels of Cp_2Ni, Cp_2Co, $(C_6H_6)_2Cr$ and hydrazine. (d) *J-V* characteristics of Cp_2Ni, Cp_2Co, $(C_6H_6)_2Cr$ and N_2H_4 doped n-SWNT/p-Si PHJ solar cells. (e) Stability of N_2H_4 and Cp_2Co doped n-SWNT/p-Si PHJ solar cells. (b-e) Reproduced with permission from Ref. [53]. Copyright 2014, American Chemical Society.

3.3 Electrochemical Gating

In addition to molecular adsorption, electrochemical gating is another effective functionalization

method which could accurately tune the Fermi levels of graphene and SWNTs. The electrochemical

14

gating is typically realized by applying a gate voltage to graphene or SWNTs through conductive solution. The ions in the conductive solution could accumulate on the surface of the graphene or SWNT film, donating or extracting electrons according to the applied voltage type. The electrochemical doping of graphene is consecutive, while that of SWNTs is stepwise when the Fermi level reaches the edges of one dimensional subbands (E_{ii}).

The electrochemical gating makes it possible to investigate the effects of Fermi-level offset on the built-in potential and PCE of the nanocarbon-based PHJ solar cells. As schemed in Figure 3a, ionic liquid was added on the top surface of the SWNT/Si PHJ solar cell to realize the electrochemical gating [64, 65]. The PCE of the electrochemical gated SWNT/Si PHJ solar cell was tuned reversibly from 4% to 11%. The applied gate voltage changed the built-in potential and the SWNT film resistance, which resulted in the modulation of V_{oc} and FF of the SWNT/Si PHJ solar cell. The negative field could also reduce the SWNT/Si interface dipole, which unpinned the Fermi level of SWNTs. Moreover, the increased charge carrier density in the SWNT film could increase the depth of the depletion layer in the n-type silicon. Figure 3b shows the electrochemical gating of the SWNT/Si nanowire (SiNW) PHJ solar cell [66]. As SiNW arrays have much larger surface area than the bulk Si, the electrochemical gating exhibited remarkable tunability on the *J-V* characteristics of the SWNT/SiNW PHJ solar cells. The V_{oc} could be reversibly altered from 0.15 V to 0.58 V, which demonstrated the effectiveness of the ionic liquid-based electrochemical gating in the three-dimensional PHJ solar cells.

The electrochemical doping regime could also be realized using a graphene electrode paired with a dielectric layer (Al_2O_3) [67]. Graphene/Al_2O_3 serving as a top gate electrode could avoid optical loss in the graphene/n-GaAs PHJ solar cell due to its high transparency, as shown in Figure 3c. The applied negative gate voltage shifted the Fermi level of graphene downwards, which resulted in a higher V_{oc} of the graphene/n-GaAs PHJ solar cell. The highest V_{oc} was 0.96 V at the gate voltage of -15 V, while the

V_{oc} was 0.7 V at zero gate voltage. At the gate voltage of -15 V, the PCE of the graphene/n-GaAs PHJ solar cell reached 18.5%, which was the highest PCE value reported so far of its kind. However, this record-high PCE may need recalculation based on energy balance, as the applied field-effect gate voltage would cause extra energy consumption. Moreover, a similar control technology of gate field was applied to the graphene/p-InP PHJ solar cells [68], in which a positive gate voltage was used to shift the Fermi level of graphene upwards. It was found that with the increase of the applied positive gate voltage, the V_{oc} of the graphene/p-InP PHJ solar cell gradually increased until reaching saturation at the gate voltage of +16 V.

The electrochemical gated nanocarbon-based PHJ solar cell belongs to the emerging screen field-effect photovoltaics [69-71]. It is an improved version of the Schottky-barrier solar cell by stabilizing surface state and creating p-n junction inside the MIS solar cell. Compared with bulk metals, graphene and SWNT films could produce deeper inversion layers in the pairing semiconductors through electrochemical gating, resulting in better device performance.
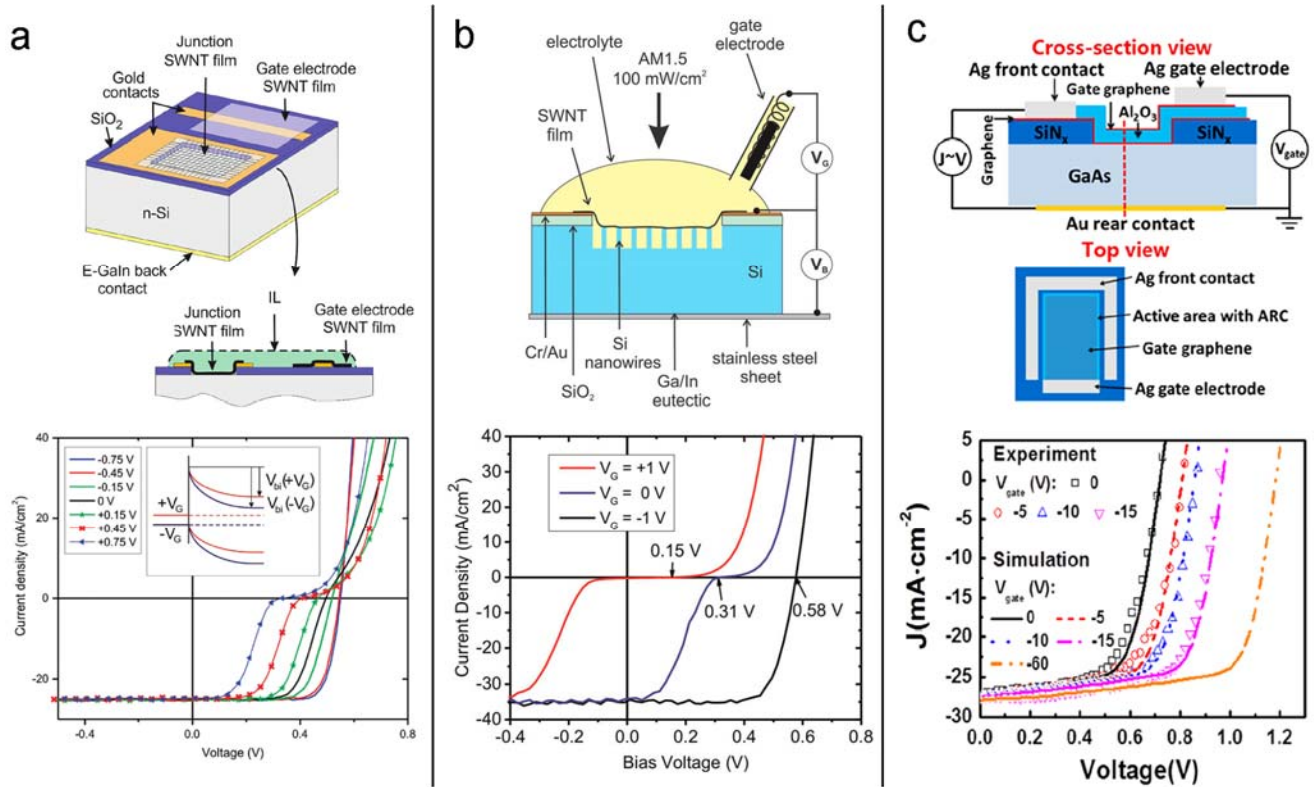
Figure 3. (a) Schematic and *J-V* curves of the SWNT/Si PHJ solar cells with ionic liquid gate electrode. Reproduced with permission from Ref. [65]. Copyright 2010, American Chemical Society. (b) Schematic and *J-V* curves of the SWNT/Si nanowire PHJ solar cells with ionic liquid gate electrode. Reproduced with permission from Ref. [66]. Copyright 2015, American Chemical Society. (c) Schematic and *J-V* curves of the graphene/n-GaAs PHJ solar cells with graphene/Al$_2$O$_3$ gate electrode. Reproduced with permission from Ref. [67]. Copyright 2015, Elsevier.

3.4 Solid-State Functionalization

   Compared with molecular adsorption and electrochemical gating, solid-state functionalization is a

more practical method for solar cells, because of its higher stability in the ambient. Low-work function

metal oxides could be thermally evaporated onto a graphene or SWNT film, followed by annealing at an

elevated temperature (140 ºC ~ 400 ºC) [72-75]. The annealing process could create non-stoichiometric

state and induce oxygen vacancies in the metal oxides. The electron traps caused by the oxygen

deficiency would extract the electrons form graphene or SWNTs and shift the Fermi level downwards

[76, 77]. Wang et al thermally deposited molybdenum oxides (MoO$_x$) onto the SWNT/Si PHJ solar cells

[13]. The MoO$_x$ layer was considered to have two main functions: as a p-dopant of SWNTs which improved the V_{oc} from 0.57 to 0.59 eV and the FF from 69% to 78%, and as an antireflection layer which improved the Jsc from 27.9 to 36.5 mA/cm^2. However, the thermal annealing effect on the performance of the SWNT/Si PHJ solar cells is unclear.

Because the solid-state dopants could not penetrate through layers of graphene or SWNT film, the solid-state functionalization usually could not achieve very high doping strength. Designing solution-based dopant precursors may be one cost-effective and scalable approach to solve this issue. Figure 4a shows a penetrative and conformal solid-state functionalization method based on redox reaction of CuCl$_2$/Cu(OH)$_2$ and SWNTs [10]. After spin-coating of CuCl$_2$/Cu(OH)$_2$ redox, the sheet resistance of the SWNT film decreased from 306.9 to 69.4 Ω/sq. immediately and did not show noticeable increase after year-long storage in the ambient. The PCE of the SWNT/Si PHJ solar cell was improved from 6.6% to 14.1% after the CuCl$_2$/Cu(OH)$_2$ redox functionalization. In addition to the p-type doping effect, the CuCl$_2$/Cu(OH)$_2$ redox was also found to unpin the Fermi level of SWNTs and enhance the charge carrier tunneling, which significantly improved the V_{oc} and FF.

The charge transfer induced by electron trap could also be realized by deposition of fluorographene [78-80] and graphene oxide quantum dots [81, 82]. In general, fluorographene and graphene oxide have relatively mild p-type doping effects on graphene and SWNTs. However, because of the homogeneous π–π stacking interactions, their applications in the nanocarbon-based PHJ solar cells are very effective and stable. By drop-casting the graphene oxide (GO) solution on top of the graphene/Si PHJ solar cells, the PCE was increased from 3.6% to 10.6% with good stability in the ambient [83]. The GO layer served as an effective p-type conductor when inserted in between graphene and Si, resulting in a deeper inversion layer [84, 85]. In addition, GO could serve as surfactant to uniformly disperse SWNTs, thereby realizing conformal doping of SWNTs [86-88]. The optimal GO/SWNT ratio was found to be

1:2.25, which was the highest SWNT concentration without precipitations after 16 hr settlement [89].

The PCE of 6.5% was achieved for the GO-dispersed SWNT/Si PHJ solar cell, which was slightly

higher than that of the pristine SWNT/Si PHJ solar cell (5.9%). Fluorinated graphene (FG) which

contains high density halogen molecules can also realize p-type solid-state doping of graphene and

SWNTs. Zhong et al [90] prepared FG by immersing pristine graphene in SF_6 plasma at 10 mTorr with a

power of 50 W and a gas feed rate of 100 sccm for 10 min. As shown in Figure 4b, after inserting FG in

between graphene and Si, both the V_{oc} and FF increased significantly, and the PCE boosted from 3.17%

to 7.52%. Moreover, the minority carrier lifetime was increased after the insertion of FG, which was

because a strong inversion layer was formed near the Si surface.

Photon-induced doping is drawing increasing attention in recent years. Constant photon exposure

could cause electron transition in graphene and SWNTs [91-93], which could be utilized to enhance the

device performance of the nanocarbon-based PHJ solar cells. Wang et al [94] observed that solar

irradiation could induce p-type doping of graphene in the graphene/Si PHJ solar cells. After 70-min

exposure to solar irradiation, a mild red-shift of the G' band in the Raman spectroscopy and a noticeable

drop in the series resistance of the graphene/Si PHJ solar cells were observed. Semiconductor quantum

dots, such as CdSe [95], InP and ZnO quantum dots [96] could also effectively cause photo-induced

charge transfer from graphene or SWNTs. Li et al [95] reported photo-induced p-type doping of

graphene by CdSe quantum dots in the graphene/h-BN/GaAs PHJ solar cells. The Schottky barrier

height of the p-doped graphene/h-BN/GaAs PHJ solar cell was 1.02 eV, while that of the un-doped

device was 0.88 eVs.

The photo-induced n-type doping of graphene and SWNTs is more challenging to be achieved,

considering their sensitivity to the ambient environment. Photo-induced electron transfer is an effective

method to overcome the p-type doping effect of ambient. Ho et al [97] observed light-induced n-type

doping of graphene, in which the inherent oxygen deficiencies of a non-stoichiometric amorphous TiO_x thin film acted as effective hole-trapping centers in gap states. The holes in the photoexcited electron–hole pairs could be trapped in gap states, while electrons in the conduction band (CB) of the TiO_x film could be transferred to graphene according to the band alignment [97]. As shown in Figure 4c, 5-min sunlight illumination on the graphene/TiO_x layer slowly shifted the Fermi level of graphene upwards and increased the PCE of the graphene/p-Si PHJ solar cell from 2.2% to 8.2% [98]. The absorption of the near-UV light by the TiO_x layer generated photo-excited electrons which were subsequently injected to graphene, resulting in n-type doping and the increased built-in potential in the graphene/p-Si PHJ solar cells.
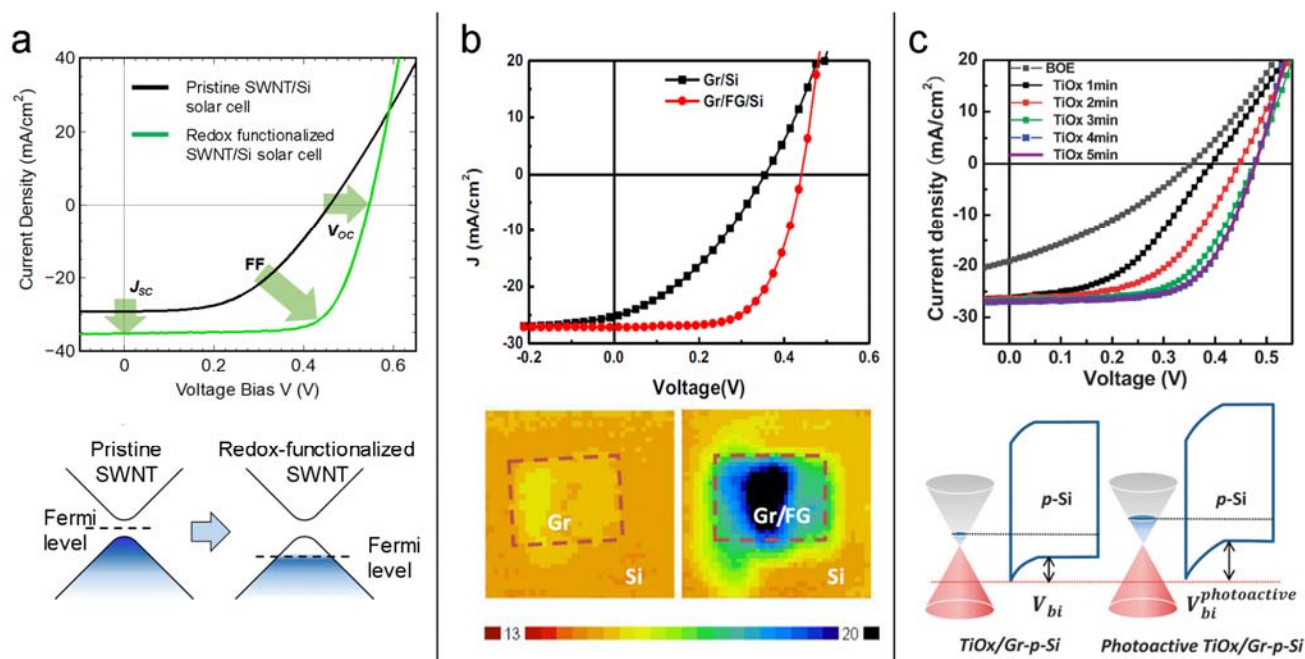

Figure 4. (a) *J-V* characteristics and mechanism of the redox functionalized SWNT/Si PHJ solar cell. Reproduced with permission from Ref. [10]. Copyright 2017, John Wiley & Sons. (b) *J-V* characteristics and carrier life time mapping of the reference graphene/Si and graphene/fluorographene/Si PHJ solar cells. Reproduced with permission from Ref. [90]. Copyright 2016, Elsevier. (c) *J-V* charecterics and band structure of photoactive TiO_2-doped graphene/Si PHJ solar cells. Reproduced with permission from Ref. [98]. Copyright 2015, Royal Society of Chemistry.

4. Electrical Property Tuning

4.1 Morphological Design and Hybrid Structure

As SWNTs are one-dimensional materials, the intra-tube electron transport along the SWNT longitudinal axis is much more efficient than that across the inter-nanotube junction. The anisotropic characteristic could be utilized through morphological design to decouple the optical transparency and electrical conductivity of SWNT films. For example, the horizontally aligned SWNTs could maintain the superior one-dimensional transport to the largest extent. Generally, the fabrication methods for the horizontally aligned SWNTs can be categorized into dry and wet processes. Figure 5a shows a typical dry process, in which the horizontally aligned MWNT film was realized by drawing the vertically aligned MWNT arrays [99]. The film was then transferred onto a patterned n-Si substrate followed by ethanol vapor treatment for film densification [100]. Compared with the randomly oriented MWNT film, the horizontally aligned MWNT film showed better contact quality with the silicon substrate. As a result, the PCE of the horizontally aligned MWNT/Si PHJ solar cell was 8.4%, which was much higher than that of the randomly oriented MWNT/Si PHJ solar cell (2.6%) [100]. On the other hand, in a typical wet process shown in Figure 5b, SWNTs were first dispersed using surfactant or chlorosulfonic acid, and then were drop-casted on a polished glass substrate. By compressing a polished substrate on top and manually sliding the two glass sheets in opposite direction, the horizontally aligned SWNT film was obtained by the shear stress. This method was also named as 'sliding coating method' [44, 101, 102]. This preparation method could suppress the roughness of the SWNT film and increase the contact area between SWNTs and the silicon substrate. Thus, the effective area for photo-energy conversion was increased, and the excited electron-hole carries in the Si substrate could be separated locally at the SWNT/Si interface. Both the dry and wet aligning processes could be carried out at room temperature,

and thus are suitable for a variety of solar cells and optoelectronic devices. The dry process is more cost-effective and can produce better alignment than the wet process, but it is only applicable to MWNTs which have more atomic defects and lower electrical conductivity than SWNTs. The thermophoresis-based dry process could tailor angle distribution of SWNTs during deposition [103, 104], which may be promising to design smarter SWNT structures for PHJ solar cells.

Another method to overcome the trade-off between the electrical conductivity and optical transparency of the nanocarbon-based electrodes is to create a three-dimensional hierarchical architecture of graphene or SWNTs with strategically placed dense and sparse portions. Cui et al [105] proposed a self-assembled hierarchical micro-honeycomb network of SWNTs, which was achieved by a 'water vapor treatment' method. As shown in Figure 5c, the micro-honeycomb network was composed of dense walls and a buckypaper bottom, which could simultaneously increase the optical transmittance and decrease the sheet resistance. The densely cross-linked SWNT walls in the micro-honeycomb structure acted as efficient conduction pathways to collect the charge carriers generated from the adjacent micro-honeycomb cells. The configuration significantly shortened the carrier diffusion path, resulting in the decreased device series resistance and increased FF value. Another hierarchical SWNT film which was composed of sub-10-μm micro-grids and random network was formed by a patterned flow deposition of SWNTs [106]. Through optimizing the thickness, width and periodicity of the SWNT grids, the sheet resistance of the hierarchical SWNT film was reduced to 53 Ω/sq. at 80% transmittance, which was 46% lower than that of the random network. Shi et al[107] applied an improved concept to the PHJ solar cells with the densified CNT grids. Figure 5d illustrates a hierarchical CNT structure composed of many capillary-densified CNT strips on top of a highly transparent CNT thin film [107]. The densified CNT strips were formed by drawing CNT films out of ethanol with a tweezer. The CNT strips only covered a small portion of the solar cell surface, with most of the active area remaining

transparent. A PCE value as high as 10% was achieved for a large-area (> 2 cm^2) CNT/Si PHJ solar cell for the first time.

Moreover, many hybrid structures were developed to increase the electrical conductivity of the nanocarbon-based electrodes. A hierarchical CNT-embroidered graphene film formed by directly transferring a CNT film onto a smooth graphene was reported by Shi et al [108]. The bi-continuous structure consist of an interconnected CNT spider-web uniformly embedded in the graphene film, resulting in co-existence of CNT/Si and graphene/Si junctions (Figure 5e). By anti-reflection coating and nitric acid doping, a PCE of 15.2% was achieved. The synergy between the highly conductive CNTs and the ultra-smooth graphene contributed to the improved device performance. Figure 5f shows the hybrid structure of the SWNT film and the Ag nanowires (AgNWs). After the hybridization, the electrical conductivity was significantly increased with a slight decrease of the optical transparency [109]. A PCE of greater than 10% was achieved for a 49 mm^2-sized AgNW-SWNT/Si PHJ solar cell. Monolayer graphene films usually suffered from minor cracks on copper growth substrates, which significantly degraded electrical conductivity [110]. The minor cracks could be filled by coating HAuCl$_4$ on top of graphene (Figure 5g) [111]. The Au filling effectively reduced the sheet resistance of the graphene film, resulting in a PCE of 12.3%. Wadhwa et al reported that the combination of the SWNT wide-spaced grid and ionic liquid (1-ethyl-3-methylimidazolium bistrifluoromethylsulfonyl)imide (EMI-BTI)) enabled more light to reach the SWNT/Si interface and created a deeper inversion layer near the interface.[64] Other conductive organic materials such as poly(3-hexylthiophene) (P3HT) [112, 113], 2,2',7,7'-tetrakis(N,N'-di-p-methoxyphenylamine)-9,9'-spirobifluorene (spiro-OMeTAD) [114, 115] and polyvinyl alcohol(PVA)-based solid electrolyte [116] were also used to realize high-performance hybrid structures for the graphene-based and SWNT-based PHJ solar cells.
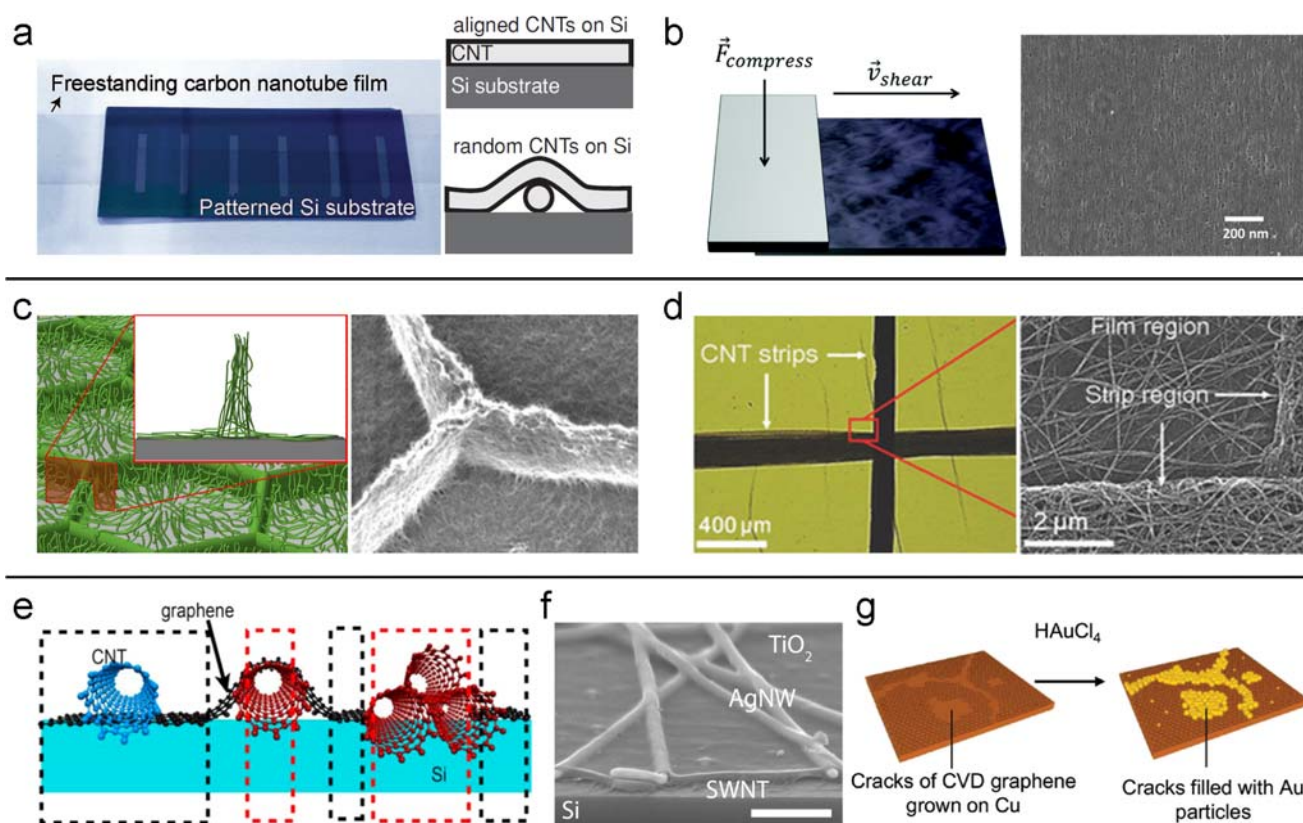
Figure 5. (a) Preparation of the horizontally aligned CNT film and the CNT/Si PHJ solar cells, as well as the schematics of the CNT/Si PHJ solar cells using aligned and random CNT films. Reproduced with permission from Ref. [100]. Copyright 2013, John Wiley & Sons. (b) Schematic of the dry-shearing process and the SEM image of the horizontally aligned SWNT film. Reproduced with permission from Ref. [102]. Copyright 2016, Royal Society of Chemistry. (c) Schematics and SEM image of the self-assembled micro-honeycomb SWNT network. Reproduced with permission from Ref. [105]. Copyright 2013, American Chemical Society. (d) Optical microscopic and SEM images of the surface morphology of the CNT film covered by densified CNT strips. Reproduced with permission from Ref. [107]. Copyright 2016, John Wiley & Sons. (e) Schematic of the CNT embroidered graphene/Si PHJ solar cells. The black and red box denote graphene/Si and CNT/Si junctions, respectively. Reproduced with permission from Ref. [108]. Copyright 2015, Elsevier. (f) SEM image of AgNWs on top of the SWNT/Si PHJ solar cell. The scale bar is 500 nm. Reproduced with permission from Ref. [117]. Copyright 2014, John Wiley & Sons. (g) Schematic of $HAuCl_4$ crack-filling for graphene on the Cu substrate. Reproduced with permission from Ref. [111]. Copyright 2015, John Wiley & Sons.

4.2 Junction Interface Engineering

Unlike the traditional semiconductor p-n junction solar cells, the nanocarbon-based PHJ solar cells are

formed by simple transfer processes of graphene or SWNT films on photoactive materials at room

temperature. This not only saves a significant amount of total energy consumption in solar cell manufacturing, but also enables in-depth investigation of interface mechanisms and exploration of innovative PHJ solar cells. The dielectric layer between nanocarbon and photoactive layers is of vital importance for alleviating Fermi level pinning and carrier recombination in PHJ solar cells.

The interfacial oxide layer in a typical Si-based PHJ solar cell was composed of a SiO_2 layer sandwiched by two layers of sub-nanometer-thick nonstoichiometric SiO_x. Oxidizing agents could penetrate through grain boundaries of graphene and inter-tube space of SWNTs to modify the thickness of the native oxide layer on Si in the nanocarbon/Si PHJ solar cells. Interestingly, previous studies on interfacial native oxide layer showed contradictory results. Jia et al [118] found that the PCE of the CNT/Si PHJ solar cell increased significantly with the growth of the native oxide layer at the interface between the CNT film and Si substrate, from 0.5% without interfacial oxide to 8.8% with an optimal oxide thickness of *ca*. 1 nm. As shown in Figure 6a, the *J-V* characteristics of the CNT/Si PHJ solar cell were highly reversible with the growth (treated by HNO_3) and removal (treated by HF) of the silicon oxide layer. The presence of the optimal oxide layer (*ca*. 1 nm-thick) could suppress the reverse saturation current and lead to a mixture of thermionic and tunneling carrier transport [118]. On the other hand, Jung et al [44] observed that the PCE of the p-SWNT/n-Si PHJ solar cell was increased after the removal of the silicon oxide layer by HF treatment, and the ideality factor of the device was approaching unity. It was also reported that the removal of the interfacial oxide by HF treatment could significantly improve the performance of the n-SWNT/p-Si PHJ solar cells [119]. The above-discussed contradictory results require further study to solidify the role of the interfacial oxide layers in the nanocarbon-based PHJ solar cells.

In recent years, angle-resolved X-ray photoemission spectroscopy (AR-XPS) was used to quantitatively investigate the effect of the interfacial oxide. The interfacial states demonstrated by the

AR-XPS spectra could be directly linked to the *J-V* characteristics of the nanocarbon/Si PHJ solar cells [120]. Based on the AR-XPS characterization, the optimal thickness of the interfacial oxide layer was 0.7 nm for the PHJ solar cells with pristine graphene or SWNT films [12, 40]. As shown in Figure 6b, a thicker oxide layer between the SWNT film and the Si substrate resulted in the hysteresis between the forward and reverse scans of the SWNT/Si PHJ solar cell, owing to the charging and discharging of the dielectric layer [40]. Doping could enhance tunneling of charge carriers and suppress recombination of electrons and holes, which increased the optimal thickness of the interfacial oxide layer to 1.5 nm [12], as shown in Figure 6c. This suggests that a heavier doping combined with a thicker interfacial oxide layer could lead to higher device performance of the nanocarbon/Si PHJ solar cells. It was also reported that RCA treatment was a powerful tool to achieve thicker interfacial oxide layers in the SWNT/Si PHJ solar cells [40]. As shown in Figure 6d, after the p-type doping process using $CuCl_2/Cu(OH)_2$, the PCE of the SWNT/Si PHJ solar cell treated by RCA for 3 min was significantly improved by 148% [10]. The increased interfacial oxide layer in the SWNT/Si PHJ solar cell could eliminate the surface states and unpin the Fermi level, boosting the p-type doping effect of $CuCl_2/Cu(OH)_2$ [40].
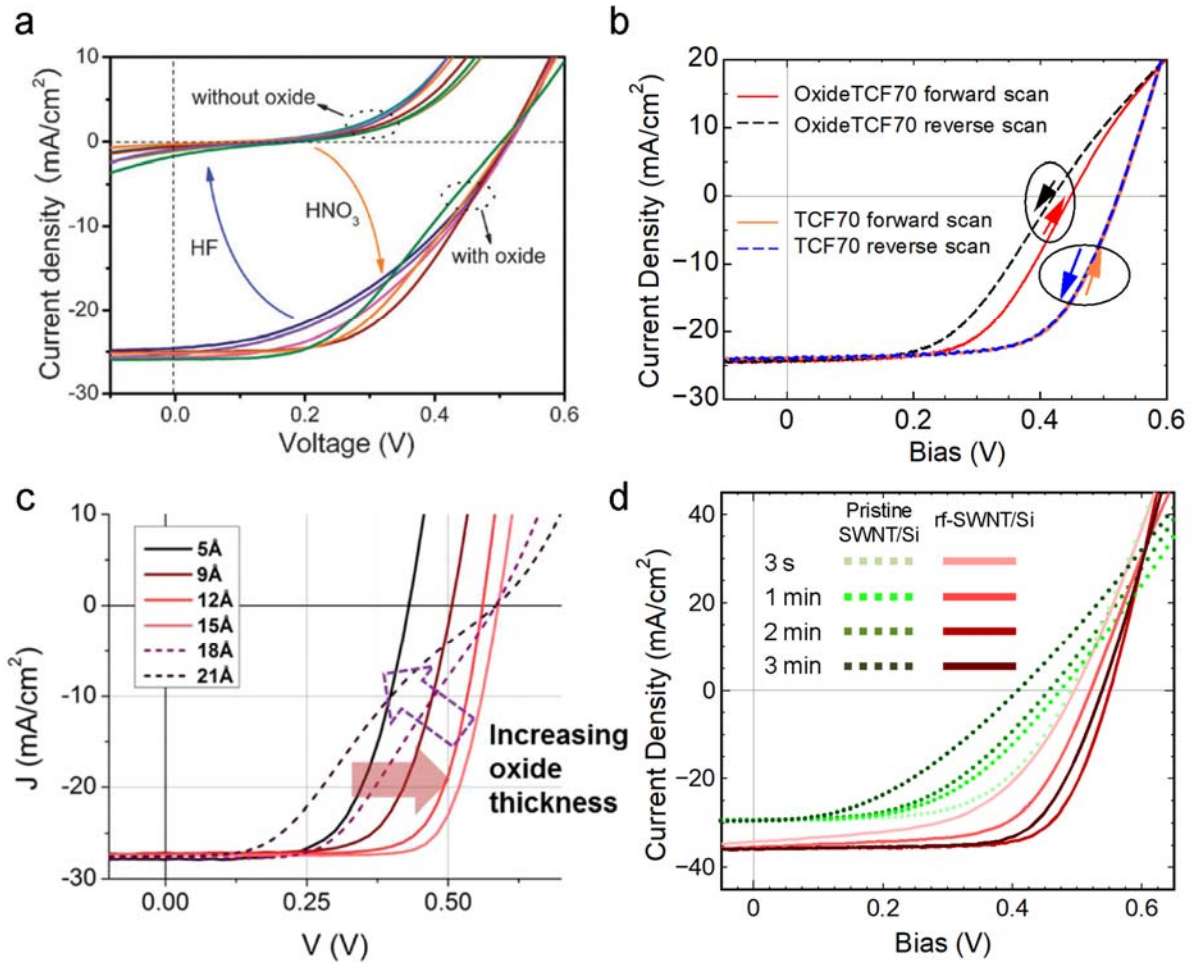
Figure 6. (a) *J–V* characteristics of the CNT/Si PHJ solar cell alternatively treated by HF and HNO_3 vapors for 6 cycles. Reproduced with permission from Ref. [118]. Copyright 2012, Royal Society of Chemistry. (b) Hysteresis of the forward and reverse scans for the SWNT/Si PHJ solar cells which have oxide layers with thicknesses of around 15 Å and 7 Å between the SWNT films and Si substrates. Reproduced with permission from Ref. [40]. Copyright 2014, Royal Society of Chemistry. (c) *J–V* characteristics of the graphene/n-silicon PHJ solar cells with varying oxide thicknesses after HNO_3 doping. Reproduced with permission from Ref. [12]. Copyright 2015, American Chemical Society. (d) *J–V* characteristics of the SWNT/Si PHJ solar cells with different RCA treatment duration before and after $CuCl_2$/$Cu(OH)_2$ redox functionalization. Reproduced with permission from Ref. [10]. Copyright 2017, John Wiley & Sons.

In addition, the emerging two-dimensional materials, such as hexagonal boron nitride (h-BN) [121-123] and molybdenum disulfide (MoS_2) [124-126], could be utilized as interfacial layers to enhance the performance of PHJ solar cells. As shown in Figure 7a, the graphene/h-BN/Si PHJ solar cell was

fabricated by transfer deposition of h-BN in between graphene and Si [127]. The PCE value of the graphene/h-BN/Si PHJ solar cell was 20% higher than that of the graphene/Si PHJ solar cell. Considering the metallic behavior of graphene, h-BN served as an effective electron-blocking/hole-transporting layer, which suppressed the interface recombination. The thickness of the h-BN layer could be tuned with atomic precision. The main advantage of the h-BN layer over the native oxide layer was that h-BN had a similar lattice constant with graphene and an atomically smooth surface without dangling bonds nor charge carrier traps [128-130], which guaranteed better contact quality with graphene. It was also reported that the insertion of MoS_2 could improve the performance of the graphene/n-Si PHJ solar cells [131, 132], although the role of MoS_2 needed further in-depth studies. Moreover, MoS_2 could be directly used as photoactive material and stacked with graphene or SWNTs to form nanocarbon/MoS_2 PHJ solar cells. These PHJ solar cells exhibiting strong photo-responsive behaviors and having PCEs of up to 1% [133-136] are comparable to the best existing ultrathin solar cells [137-139]. The vertical van der Waal stacked layer structure offers a new direction for ultralight, ultrathin and high-efficient portable solar cells.

Metal oxides with high work function, such as MoO_3, Al_2O_3, WO_3 *etc.* could be deposited in between nanocarbon and photoactive layers as interfacial materials in PHJ solar cells. Figure 7b illustrates the schematic and *J-V* curves of the graphene/WO_3/Si PHJ solar cell [140, 141]. The WO_3 thin film with the optimal thickness of 15 nm was facilely deposited on top of the Si substrate using thermal evaporation. A PCE of 10.59% was achieved for the optimized graphene/WO_3/Si PHJ solar cell, compared with 3.99% for the graphene/Si PHJ solar cell. The band structure (Figure 7b) illustrated the large offset between the Fermi-levels of WO_3 and Si, which resulted in upward band bending at the WO_3/Si interface and enhanced built-in potential. The WO_3/Si interface also acted as an electron-blocking layer for selective hole transport toward graphene.

Interface engineering between the graphene-based or SWNT-based electrode and the photoactive semiconductor is not only an effective way to improve the PHJ solar cell performance, but also a platform to investigate fundamental semiconductor physics such as Fermi level pinning [142]. Moreover, the interfaces with multi-functions reviewed here are also promising to be applied in the organic solar cells [143], organic-inorganic perovskite solar cells [144], and other optoelectronic devices such as light-emitting diodes [145] and photodetectors [146].
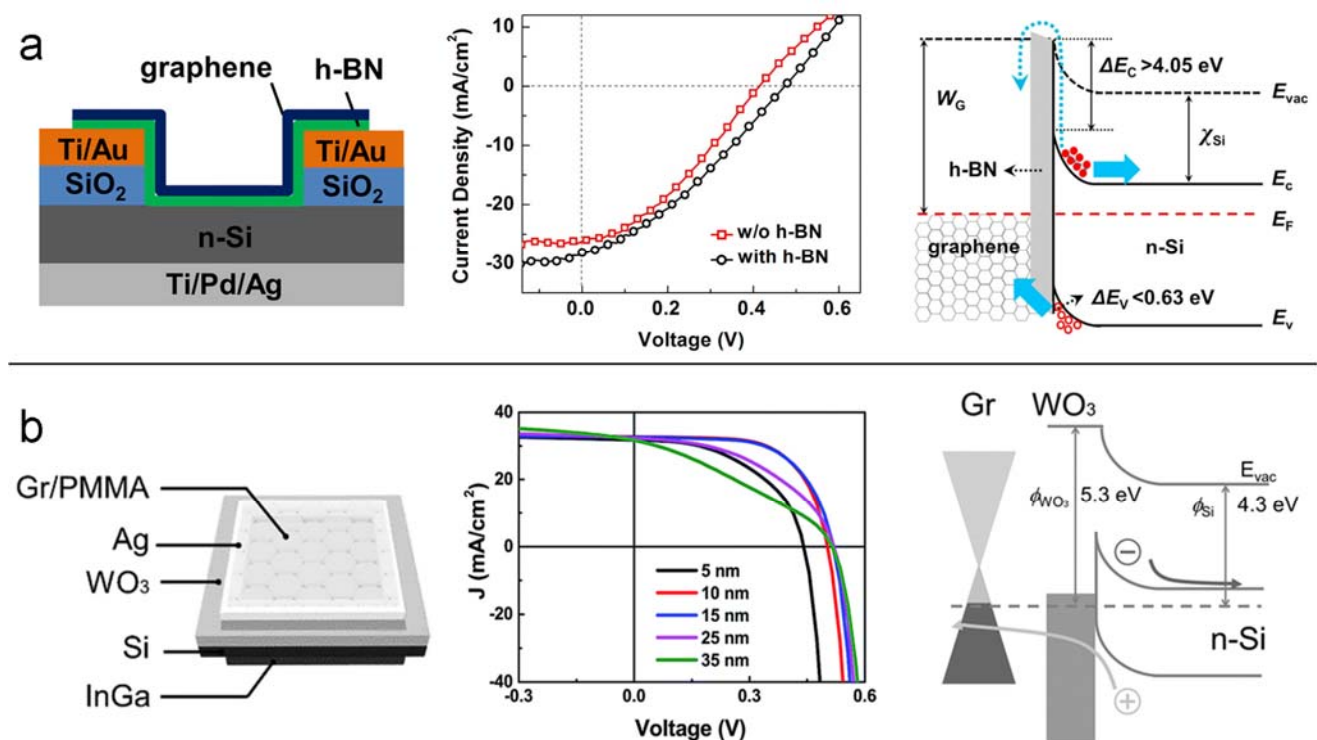

Figure 7. (a) Schematic, *J-V* curves and electronic band structure of the graphene/h-BN/Si PHJ solar cell. Reproduced with permission from Ref. [127]. Copyright 2016, Elsevier. (b) Schematic, *J-V* curves and electronic band structure of the graphene/WO₃/Si PHJ solar cell. Reproduced with permission from Ref. [140]. Copyright 2016, Royal Society of Chemistry.

5. Optical Property Tuning

5.1 Antireflection Coating

For PHJ solar cells, the light reflection from the polished surface of the crystalline Si or GaAs could be more than 30% [147], which caused substantial energy loss in the light absorption. Antireflection structures such as honeycomb texture [147] pyramid texture [148, 149] black silicon [150-152] as well as vertical arrays of semiconducting nanowires [153] could reduce light reflection effectively. However, these antireflection structures are usually fabricated by photolithography and reactive ion etching of the crystalline semiconductor surfaces. Alternatively, the antireflection coating (ARC) can be deposited through a scalable method which is promising for the graphene-based and SWNT-based PHJ solar cells.

TiO$_2$ with a refractive index of 2.2 could generate destructive interference at the air-TiO$_2$ junction, which would trap the incident light in a certain wavelength range. The condition for the full destructive interference is given as d = λ / (4·n), where d is the thickness of the ARC, λ is the wavelength of the incident light, and n is the refractive index of the ARC. The schematic of the antireflection effect of the TiO$_2$ layer caused by the destructive interference is shown in Figure 8a [154]. It is preferable to have low reflectance in the wavelength range of 400 – 800 nm (major solar irradiance). Both full and partial destructive interferences can decrease the reflectance. It was reported that a 70-nm-thick coating layer of the colloidal TiO$_2$ nanoparticles decreased the light reflectance of the CNT/Si PHJ solar cell from *ca*. 40% to less than 5% at the wavelength of 600 nm (Figure 8b), resulting in the significant increase of J_{sc}.[12, 154, 155] Molybdenum oxide (MoO$_x$) was also an effective ARC material which could reduce the light reflectance from *ca*. 35% to *ca*. 20% [156]. In the wavelength range of 400 – 1200 nm, the light reflectance of the MoO$_x$-SWNT/Si PHJ solar cell (Figure 8c) did not show an interference pattern, owing to the non-stoichiometric composition of MoO$_x$ with a relatively broad refractive index.

Polymer materials, such as polymethylmethacrylate (PMMA) [157] and poly (3, 4-ethylene dioxythiophene):poly (styrenesulfonate) (PEDOT:PSS) [158, 159], could also be applied as ARC materials through spin-coating to increase PCEs of the nanocarbon-based PHJ solar cells, as shown in Figure 8d and 8e. Their thicknesses could be modulated by changing the concentration of the solutions. In addition, PMMA could block the ambient environment and extend the doping effect of nitric acid on the CNT/Si PHJ solar cells [157]; while PEDOT:PSS could reduce the series resistance of the CNT/Si PHJ solar cells [158]. Moreover, the colloidal $CuCl_2/Cu(OH)_2$ redox, which served as both ARC and p-type dopant to SWNT films, was a multifunctional coating material for the SWNT/Si PHJ solar cells [10]. A 50% decrease of the light reflection of the SWNT/Si PHJ solar cell as well as a five-fold sheet resistance decrease of the SWNT film were realized by using a 30-nm-thick $CuCl_2/Cu(OH)_2$ redox coating layer, as shown in Figure 8f.
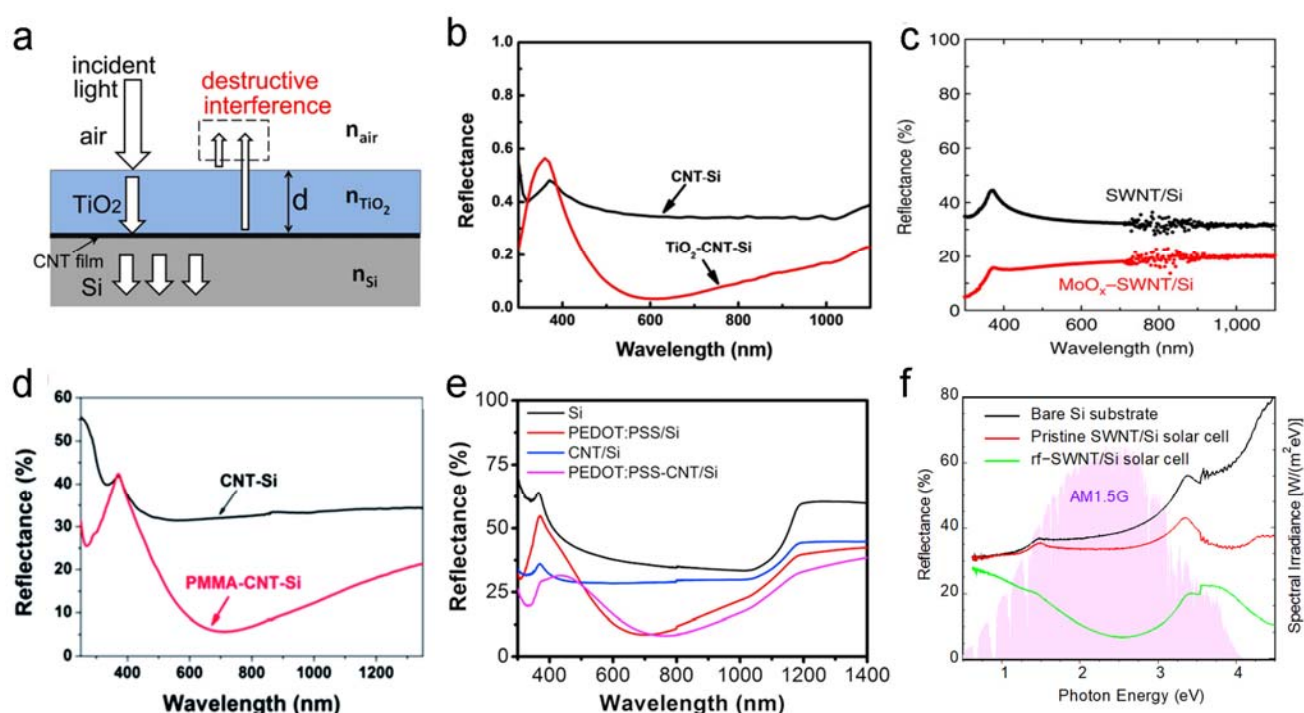

Figure 8. (a) Schematic of antireflection effect of the TiO_2 layer caused by destructive interference. (b) Reflectance spectra of CNT/Si PHJ solar cells with and without TiO_2 coating. (a, b) Reproduced with

permission from Ref. [154]. Copyright 2012, Nature Publishing Group. (c) Reflectance spectra of SWNT/Si PHJ solar cells with and without MoO$_x$. Reproduced with permission from Ref. [13]. Copyright 2015, Nature Publishing Group. (d) Reflectance spectra of CNT/Si PHJ solar cells with and without PMMA coating. Reproduced with permission from Ref. [157]. Copyright 2014, Royal Society of Chemistry. (e) Reflectance spectra of CNT/Si PHJ solar cells with and without PEDOT:PSS coating. Reproduced with permission from Ref. [158]. Copyright 2017, Elsevier. (f) Reflectance spectra of SWNT/Si PHJ solar cells with and without CuCl$_2$/Cu(OH)$_2$ coating. Reproduced with permission from Ref. [10]. Copyright 2017, John Wiley & Sons.

5.2 Plasmonic-Enhanced Absorption

Localized surface plasmon resonance is the excited electron oscillation when light at the plasmon resonance frequency scatters at the surface of the metal nanoparticles (NPs). The scattering cross-section of metal NPs can be orders of magnitude larger than the physical cross-section, owing to the strong light-matter interaction [160]. Therefore, plasmon-induced light trapping has been widely used to enhance the light absorption in inorganic thin-film solar cells [161-165], organic solar cells [166-168] and organometallic perovskite solar cells [169-172]. Furthermore, the plasmon-induced electron-hole pairs could be harvested by a charge separation process, which further contributes to the photocurrent enhancement [166].

The plasmonic effect could effectively improve the performance of the graphene-based and SWNT-based PHJ solar cells. For the SWNT photodetectors [173] and SWNT/Si PHJ solar cells [174], large-diameter SWNTs have better coupling with the localized surface plasmon of NPs than small-diameter SWNTs. As shown in Figure 9a, the cubic-shaped Pt NPs with the average diameter of 7 nm were spin-coated on top of the graphene/Si PHJ solar cell. After the deposition of Pt NPs, the PCE of the graphene/Si PHJ solar cell was increased from 4.92% to 7.04%, accompanied with the increased J_{sc}, V_{oc} and FF [175]. The cubic-shaped Pt NPs could scatter a broader wavelength range of sunlight than the sphere Pt NPs, resulting in enhanced solar absorption and shorter penetration depth of the sunlight, hence greater J_{sc} values. The cubic-shaped Pt NPs with high work function p-doped graphene and

shifted its Fermi level upwards, resulting in the increased V_{oc}. Moreover, the PCE of the graphene/Si PHJ solar cell with cubic-shaped Pt NPs increased under continuous sunlight illumination,[175] which may be attributed to that the hole injection from the Si substrate neutralized the plasmon-induced hot electron injection from noble metal NPs [176, 177]. As shown in Figure 9b, after coating 80-nm-diameter sphere-shaped Au NPs on graphene, the PCE of the graphene/GaAs PHJ solar cell increased from 8.83% to 11.8% [11]. The J_{sc} was also increased significantly after Au NPs coating, but the V_{oc} and FF were remained almost the same. With the Au NPs surface plasmon, the solar absorption mainly occurred near the graphene/GaAs heterojunction (Figure 9c) where the separation and collection of charge carriers were more efficient, resulting in the increased J_{sc} [11].

To investigate the effect of the Au NPs on the light absorption in the Si substrate, Luo et al [178] used finite elemental method (FEM) to simulate the relative electric field distribution ($|E|^2 = |E_0|^2$) at the heterojunctions with and without Au NPs, as shown in Figure 9d. A hot spot with high electric field intensity was found beneath each Au NP, owing to the surface plasmon resonance. Under the optimal conditions (the lattice constant was 300 nm, and the Au NP diameter was 80 nm), the light absorption in the Si substrate was enhanced by 5.5% at the wavelength of 600 nm. The enhancement could effectively improve the PCE by limiting the charge separation near the graphene/Si heterojunction.

It is worth mentioning that graphene [179] and SWNTs [180-182] have inherent plasmon resonance absorption. Nevertheless, their inherent plasmon effect has not been utilized in PHJ solar cells so far, as the plasmonic peak positions of the graphene and SWNTs locate in the terahertz-to-far infrared and ultra-UV ranges. Through tuning of Fermi level and modification of geometrical size, the plasmonic peak positions of graphene and SWNTs can be shifted to near infrared [181-186], making it applicable to enhance the performance of the PHJ solar cells.
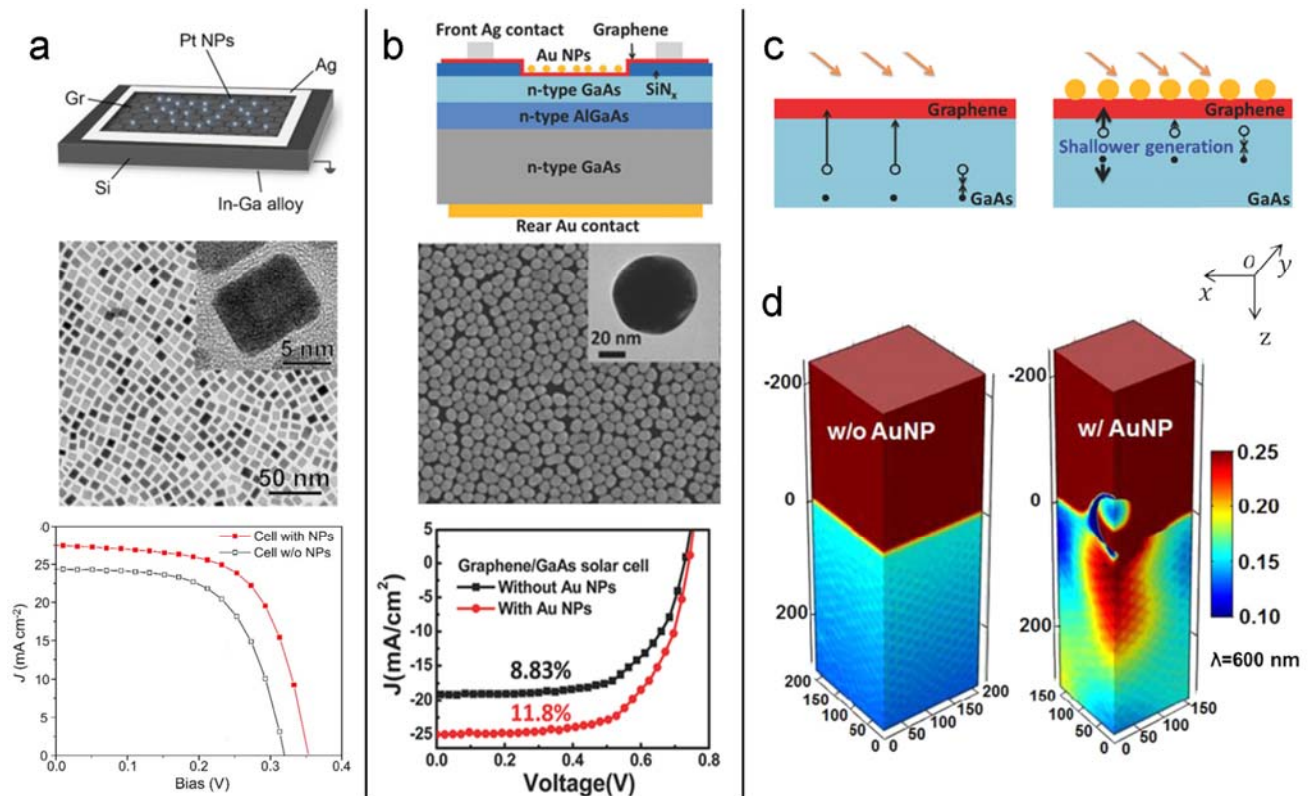
Figure 9. (a) Top: schematic diagram of the graphene/Si PHJ solar cell with Pt nanoparticles. Middle: SEM and TEM (inset) of Pt cubic nanoparticles. Bottom: comparison of *J-V* curves of the graphene/Si PHJ solar cells with and without Pt nanoparticles. Reproduced with permission from Ref. [175]. Copyright 2016, Elsevier. (b) Top: schematic diagram of the graphene/GaAs PHJ solar cell with Au nanoparticles. Middle: SEM and TEM (inset) of Au nanoparticles. Bottom: comparison of *J-V* curves of the graphene/GaAs PHJ solar cells with and without Au nanoparticles. (c) Schematics of the solar absorption and carrier kinetics in the graphene/GaAs heterojunctions without and with the Au nanoparticles. (b, c) Reproduced with permission from Ref. [11]. Copyright 2016, John Wiley & Sons. (d) Finite element simulation of electric field distribution in the Si substrates without and with Au nanoparticles under irradiation at wavelength of 600 nm. Reproduced with permission from Ref. [178]. Copyright 2014, Elsevier.

6. Towards Flexible PHJ Solar Cells

Flexible PHJ solar cells can provide portable power for ubiquitous electronic sensors and devices. The electrodes and the photoactive materials of the flexible PHJ solar cells are required to possess excellent mechanical flexibility and robustness. The superior mechanical property and electrical conductivity of graphene and SWNTs make them the perfect candidates as the electrode materials of the flexible PHJ

solar cells. Through chemical functionalization as well as smart morphological, electronic and photonic designs, the performance of the graphene-based and SWNT-based flexible PHJ solar cells is superior over that of the conventional ITO-based ones [187].

Silicon is robust, manufacturable and Earth-abundant, and thus is the most suitable photoactive material for solar cells. However, the material cost of the crystalline Si (c-Si) wafer comprises *ca*. 15% of the total PV module cost. Using c-Si thin films is an effective way to cut material cost and limit total PV module cost to below US$0.50–0.75/W, which is critical for utility-scale adoption [1-3, 188, 189]. More importantly, the c-Si film with a thickness less than 50 μm indicates good flexural rigidity, and its flexibility increases with the decrease of the film thickness [190]. However, decreasing the c-Si film thickness to below 50 μm would cause insufficient light absorption and degraded PCEs. The trade-off between the flexibility and the light absorption is major technological difficulty limiting the advancement of the flexible graphene/Si and SWNT/Si PHJ solar cells. Ruan et al fabricated flexible graphene/Si PHJ solar cells using thin c-Si films with different thicknesses (10, 20 and 40 μm) for the first time [191]. The used processes included passivation of the Si surface, poly(3-hexylthiophene) (P3HT) coating and optimization of the graphene thickness. The optimal PCEs of the graphene/10-μm-thick Si and graphene/40-μm-thick Si flexible PHJ solar cells were 2.92% and 8.42%, respectively. Figure 10a shows that the PCE of the graphene/10-μm-thick Si PHJ solar cell degraded by only 7% after 60 bending cycles at a fixed bending radius of 8 mm [192]. Figure 10b shows the recently developed kerf-less mechanical exfoliation technique to obtain ultrathin c-Si foils on the "parent" Si wafer [193]. A Nickel film with a thickness of 50–55 μm was electroplated onto the back surface of the c-Si substrate. Alternate thermal annealing and controlled spalling processes induced thermal stress at the metal/Si interface and initiated a crack at the wafer edge for the exfoliation of ultrathin c-Si film. The thickness of the exfoliated ultrathin c-Si film could be tuned by controlling the temperature of the thermal cycling

process. A PCE of 7.4% was obtained for the flexible graphene/8-μm-thick Si PHJ solar cell. The 8-μm-thick Si film was the thinnest Si substrate ever used for the fabrication of the flexible graphene/Si PHJ solar cells.

Despite the impressive mechanical robustness, the PCEs of the flexible graphene/Si PHJ solar cells were relatively low due to the insufficient solar absorption of graphene and Si. The better photon absorption of SWNTs could be the key to improve the performance of the flexible Si-based PHJ solar cells. Li et al [194] realized the flexible SWNT/Si PHJ solar cell by mounting the flexible n-type Si wafer (with a SWNT cathode on top) onto a thin PET sheet, as shown in Figure 10c. The PCEs of the flexible SWNT/12-μm-thick Si and SWNT/50-μm-thick Si PHJ solar cells without any additional light-trapping structures were 3.48% and 7.37%, respectively. The photocarrier generation in the SWNTs as well as the photocarrier injection from the SWNTs into the flexible Si film were clarified by the femtosecond transient absorption spectroscopy method. The strong light-matter interaction was induced by the quantum confinement of the SWNTs. Applying SWNTs to generate photocurrent was promising to tackle the insufficient light absorption of the flexible Si substrate.
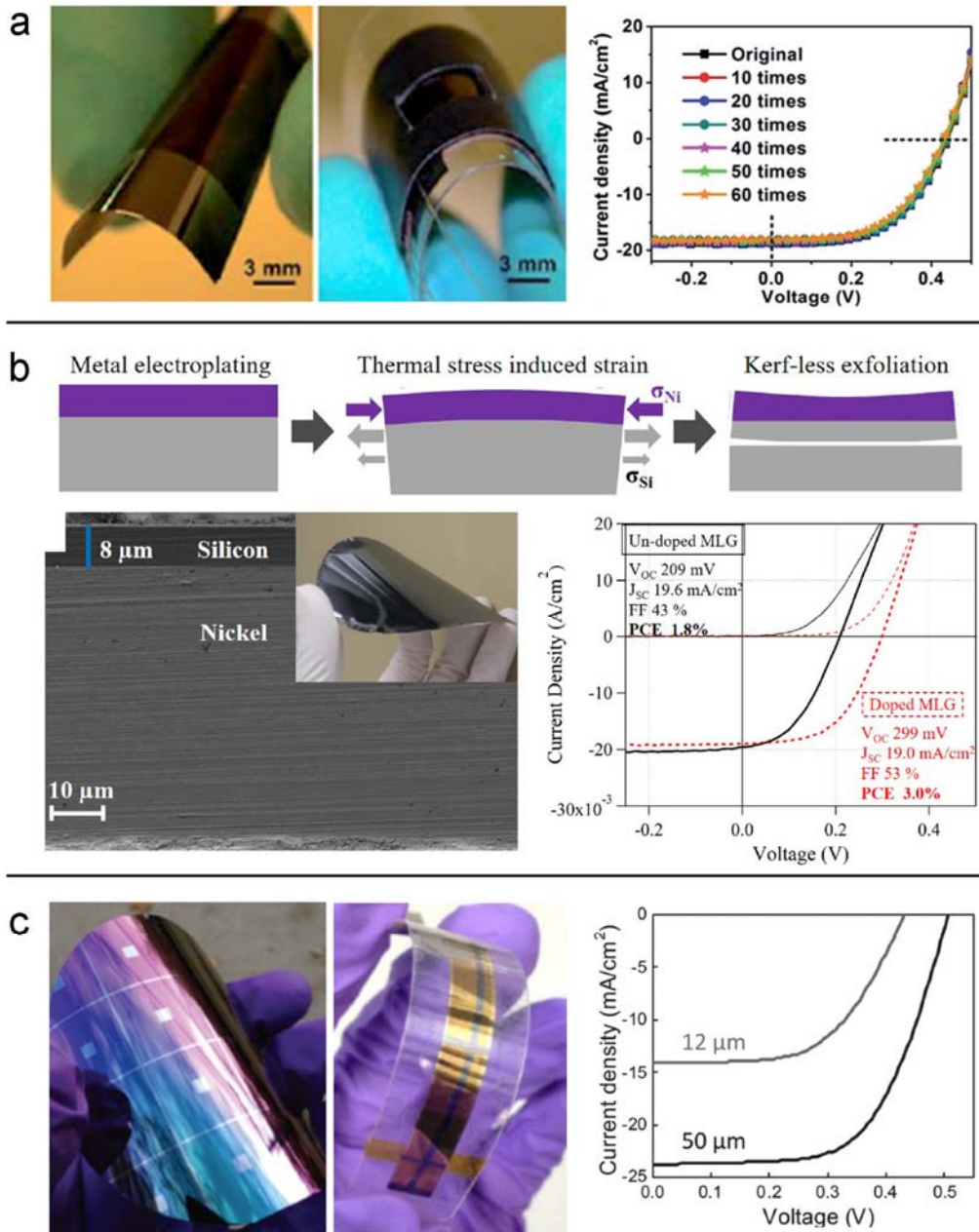
Figure 10. (a) Photographs and *J-V* characteristics of the flexible graphene/Si PHJ solar cells after different bending cycles. Reproduced with permission from Ref. [192]. Copyright 2015, Royal Society of Chemistry. (b) Schematic of kerf-less exfoliation process, photograph and SEM image of the exfoliated ultrathin c-Si film, as well as *J-V* characteristics of the flexible graphene/Si PHJ solar cells. Reproduced with permission from Ref. [193]. Copyright 2017, American Institute of Physics. (c) Photographs and *J-V* characteristics of the flexible SWNT/Si PHJ solar cells with different Si thicknesses. Reproduced with permission from Ref. [194]. Copyright 2017, John Wiley & Sons.

In addition to the flexible c-Si substrates, graphene and SWNT films can be transferred on various flexible polymer substrates, such as PEN, PET, PMMA and parylene, to realize organic or organometallic flexible PHJ solar cells [195, 196]. Normalized PCEs as a function of bending cycles at a certain bending radius are usually used to evaluate the mechanical robustness and flexural rigidity of the flexible PHJ solar cells. Yoon et al fabricated a flexible organometallic perovskite solar cell (PEDOT:PSS/Gr-Mo/PEN) through transferring the MoO_x-functionalized graphene film on the PEN substrate.[197] The reference flexible solar cell (PEDOT:PSS/ITO/PEN) used the ITO cathode and the PEN substrate. After 1000 bending cycles at a bending radius of 4 mm, an obvious crack was formed through the ITO layer and propagated into the photoactive layer in the PEDOT:PSS/ITO/PEN solar cell (Figure 11a), while the graphene film in the PEDOT:PSS/Gr-Mo/PEN solar cell remained intact (Figure 11b). As indicated in Figure 11c, owing to the occurrence of the fracture in the ITO layer, the PCE of the PEDOT:PSS/ITO/PEN solar cell deteriorated significantly from 17.3% to 4.3%, while the PCE of the PEDOT:PSS/Gr-Mo/PEN solar cell remained 90% of its original value (16.8%).

The superiorities of graphene and SWNT films over the ITO layer in terms of flexibility and mechanical robustness were also utilized in the flexible organic PHJ solar cells [143, 198]. Song et al fabricated a flexible organic PHJ solar cell (Gr/Gr) by using the MoOx-functionalized graphene film as the anode, the ZnO-functionalized graphene film as the cathode on a PEN substrate, and PDTP-DFBT:$PC_{70}BM$ as the photoactive layer. The reference flexible organic PHJ solar cells were ITO/Al (cathode is ITO, anode is Al) and ITO/Gr (cathode is ITO, anode is graphene) with the same photoactive layer. The photographs of the three organic solar cells (ITO/Al, ITO/Gr and Gr/Gr) during bending tests at bending radii of 2.0, 1.2 and 0.7 mm were shown in Figure 11d. After 1000 bending cycles at a bending radius of 1.2 mm, the normalized PCE of the Gr/Gr flexible organic PHJ solar cell remained unchanged, demonstrating the highest flexibility, as shown in Figure 11e. The excellent mechanical

properties of the graphene and SWNT films could be further exploited to realize more foldable and wearable PHJ solar cells.
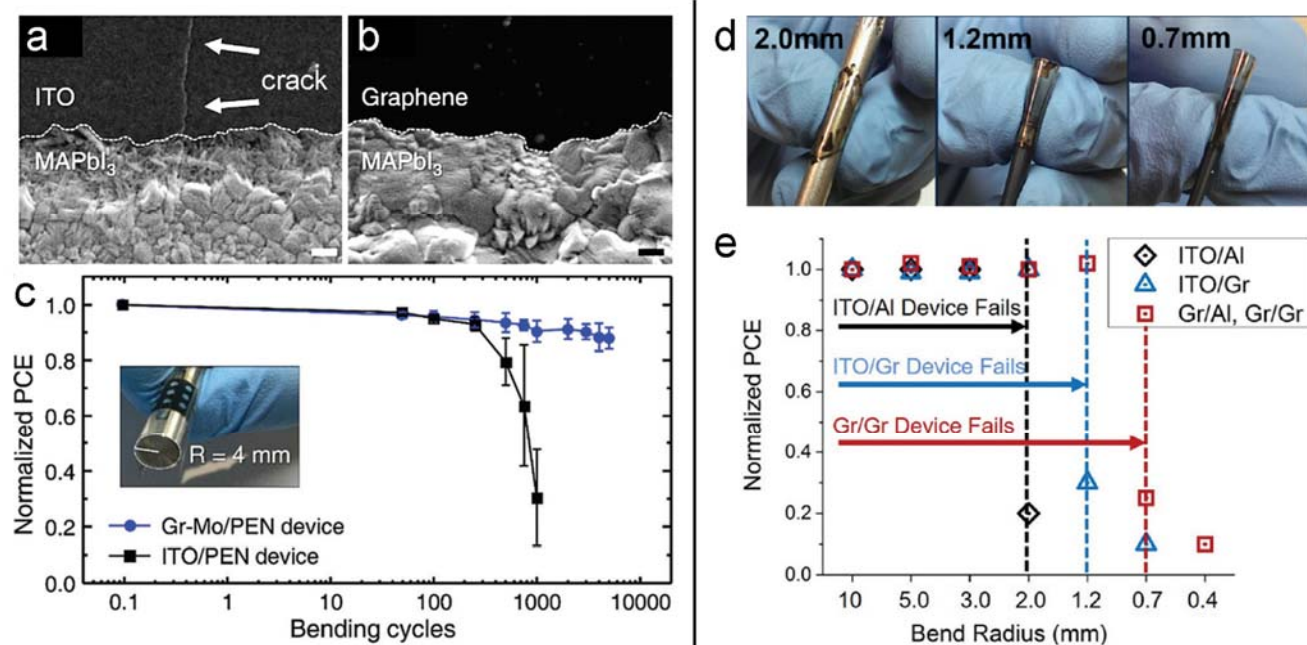

Figure 11. Plane-view SEM images of the MAPbI3 perovskite films prepared on (a) PEDOT:PSS/ITO/PEN and (b) PEDOT:PSS/Graphene-MoOx/PEN films, measured after 1000 bending cycles at a fixed bending radius of 4 mm (scale bar: 200 nm). (c) Normalized PCEs of the flexible PEDOT:PSS/ITO/PEN and PEDOT:PSS/Graphene-MoOx/PEN PHJ solar cells as a function of bending cycle at a fixed bending radius of 4 mm. (a, b, c) Reproduced with permission from Ref. [197]. Copyright 2017, Royal Society of Chemistry. (d) Photographs of the flexible organic PHJ solar cells using different cathode/anode pairs (ITO/Al, ITO/Gr and Gr/Gr) after bending tests at the curvature radii of 2.0, 1.2 and 0.7 mm, respectively. (e) Normalized PCEs of the flexible organic PHJ solar cells using different cathode/anode pairs (ITO/Al, ITO/Gr and Gr/Gr) as a function of bending radius. (d, e) Reproduced with permission from Ref. [198]. Copyright 2016, John Wiley & Sons.

7 Future Prospects

Photovoltaics are expected to be market-competitive and subsidy-free utility-scale adoption at module costs of US$0.50–0.75 per peak watt (W_p), which results in a levelized cost of electricity (LCOE) of US$0.06/kWh, similar to the current fossil fuel-based electrical utility plants. Currently, estimated

manufacturing cost of c-Si PV is US$1.29/Wp for a US manufacturer, which is two to three times higher than the US$0.50/$W_p$ target. The c-Si photovoltaics are robust, manufacturable and Earth-abundant. Based on the above discussions, graphene and carbon nanotubes are promising enabling technologies to reduce Si feedstock utilization as well as realize higher PCEs using thinner wafers and simplified cell architectures.

As of 2017, the highest PCE is 26.3% for the c-Si PHJ solar cell which utilizes a p-type amorphous Si (p:a-Si) layer and a n-type amorphous Si (n:a-Si) layer patterned to collect holes and electrons, respectively [9]. Although the PCEs of the graphene-based and CNT-based PHJ solar cells have rocketed to 14 – 17% in a short period, there is still plenty of room to further improve the device performance by optimizing the preparation and deposition processes of graphene and CNTs. Moreover, the mechanical flexibility of graphene and CNTs has not been exploited to its full extent. With few researches so far, the PCEs of the flexible nanocarbon-based PHJ solar cells have already achieved 8.42%, which is at the forefront of all the flexible PHJ solar cells. We expect flexible graphene-based and CNT-based PHJ solar cells with PCEs over 15% could be realized in the near future, which would play a great role as ubiquitous power supply for portable electronic products such as smart phones, wearable devices and internet of things.

8 Summary

The development of graphene-based and CNT-based PHJ solar cells relies on the synergistic progress of preparation and functionalization of nanocarbon films, as well as design and fabrication of PHJ solar cells. In this review, we have summarized the key strategies to improve the potential for practical and scalable deployment of the graphene-based and CNT-based PHJ solar cells. At the nanoscale, the Fermi level of graphene and CNTs can be shifted to increase carrier mobility and built-in potential, which facilitates selective charge transport and separation. Fermi level tuning of graphene and CNTs can be

realized through molecular adsorption, electrochemical gating and solid-state functionalization. By appropriate functionalization process, the graphene/CNT top electrode layer could be paired with either p-type or n-type photoactive layer to form PHJ solar cells, which offers flexible design of novel solar cell structures. At the microscale, the morphologies of graphene and CNTs could be modified to efficiently organize charge separation and transport near the interface. Design and fabrication of three-dimensional hierarchical architectures of graphene and CNTs could decouple electrical and optical conductivities, which overcomes the trade-off for TCFs. Hybrid or composite structures of graphene/CNTs with other materials could also achieve multi-functionalization and improve PCEs. At the macroscale, device level optimization was mostly inspired by the accumulated technological know-how of Si-based and GaAs-based solar cells. Tuning of interfacial oxide thickness and insertion of atomic-thin 2D materials could effectively change the band alignment to prevent Fermi level pinning and charge carrier recombination. For light management, the ARC could effectively harvest light reflection, while plasmonic effect could confine the solar absorption near the interface. With sophistication of carbon nanomaterials and its integration with current c-Si and GaAs production technology, we believe that nanocarbon-based PHJ solar cells will soon have an impact on global energy production at the terawatt scale.

Reference

[1] Powell DM, Fu R, Horowitz K, Basore PA, Woodhouse M, Buonassisi T. The capital intensity of photovoltaics manufacturing: barrier to scale and opportunity for innovation. Energy Environ Sci. 2015;8:3395-3408.
[2] Powell DM, Winkler MT, Choi HJ, Simmons CB, Needleman DB, Buonassisi T. Crystalline silicon photovoltaics: a cost analysis framework for determining technology pathways to reach baseload electricity costs. Energy Environ Sci. 2012;5:5874-5883.
[3] Tomasi A, Paviet-Salomon B, Jeangros Q, Haschke J, Christmann G, Barraud L, et al. Simple processing of back-contacted silicon heterojunction solar cells using selective-area crystalline growth. Nature Energy. 2017;2:17062.

[4] Campoy-Quiles M, Ferenczi T, Agostinelli T, Etchegoin PG, Kim Y, Anthopoulos TD, et al. Morphology evolution via self-organization and lateral and vertical diffusion in polymer:fullerene solar cell blends. Nature Mater. 2008;7:158.

[5] Christians JA, Schulz P, Tinkham JS, Schloemer TH, Harvey SP, Tremolet de Villers BJ, et al. Tailored interfaces of unencapsulated perovskite solar cells for >1,000 hour operational stability. Nature Energy. 2018;3:68-74.

[6] Correa-Baena J-P, Saliba M, Buonassisi T, Grätzel M, Abate A, Tress W, et al. Promises and challenges of perovskite solar cells. Science. 2017;358:739-744.

[7] Green MA, Ho-Baillie A, Snaith HJ. The emergence of perovskite solar cells. Nature Photon. 2014;8:506.

[8] Li M, Gao K, Wan X, Zhang Q, Kan B, Xia R, et al. Solution-processed organic tandem solar cells with power conversion efficiencies >12%. Nature Photon. 2016;11:85.

[9] Yoshikawa K, Kawasaki H, Yoshida W, Irie T, Konishi K, Nakano K, et al. Silicon heterojunction solar cell with interdigitated back contacts for a photoconversion efficiency over 26%. Nature Energy. 2017;2:17032.

[10] Cui K, Qian Y, Jeon I, Anisimov A, Matsuo Y, Kauppinen EI, et al. Scalable and Solid-State Redox Functionalization of Transparent Single-Walled Carbon Nanotube Films for Highly Efficient and Stable Solar Cells. Adv Energy Mater. 2017;7:1700449-n/a.

[11] Lin S-S, Wu Z-Q, Li X-Q, Zhang Y-J, Zhang S-J, Wang P, et al. Stable 16.2% Efficient Surface Plasmon-Enhanced Graphene/GaAs Heterostructure Solar Cell. Adv Energy Mater. 2016;6:1600822-n/a.

[12] Song Y, Li X, Mackin C, Zhang X, Fang W, Palacios T, et al. Role of Interfacial Oxide in High-Efficiency Graphene–Silicon Schottky Barrier Solar Cells. Nano Lett. 2015;15:2104-2110.

[13] Wang F, Kozawa D, Miyauchi Y, Hiraoka K, Mouri S, Ohno Y, et al. Considerably improved photovoltaic performance of carbon nanotube-based solar cells using metal oxide layers. Nature Commun. 2015;6.

[14] Ribeyron P-J. Crystalline silicon solar cells: Better than ever. Nature Energy. 2017;2:17067.

[15] Kojima A, Teshima K, Shirai Y, Miyasaka T. Organometal Halide Perovskites as Visible-Light Sensitizers for Photovoltaic Cells. J Am Chem Soc. 2009;131:6050-6051.

[16] Yang WS, Park B-W, Jung EH, Jeon NJ, Kim YC, Lee DU, et al. Iodide management in formamidinium-lead-halide–based perovskite layers for efficient solar cells. Science. 2017;356:1376-1379.

[17] Chen HN, Wei ZH, He HX, Zheng XL, Wong KS, Yang SH. Solvent Engineering Boosts the Efficiency of Paintable Carbon-Based Perovskite Solar Cells to Beyond 14%. Adv Energy Mater. 2016;6.

[18] Kim J, Yun JS, Cho Y, Lee DS, Wilkinson B, Soufiani AM, et al. Overcoming the Challenges of Large-Area High-Efficiency Perovskite Solar Cells. ACS Energy Lett. 2017;2:1978-1984.

[19] Babayigit A, Ethirajan A, Muller M, Conings B. Toxicity of organometal halide perovskite solar cells. Nature Mater. 2016;15:247.

[20] Yang Z, Chueh CC, Zuo F, Kim JH, Liang PW, Jen AKY. High‐Performance Fully Printable Perovskite Solar Cells via Blade‐Coating Technique under the Ambient Condition. Adv Energy Mater. 2015;5:1500328.

[21] Chen J, Rong Y, Mei A, Xiong Y, Liu T, Sheng Y, et al. Hole‐Conductor‐Free Fully Printable Mesoscopic Solar Cell with Mixed‐Anion Perovskite CH3NH3PbI(3−x)(BF4)x. Adv Energy Mater. 2016;6:1502009.

[22] Cai M, Wu Y, Chen H, Yang X, Qiang Y, Han L. Cost‐Performance Analysis of Perovskite Solar Modules. Adv Sci. 2017;4:1600269.

[23] Morozov SV, Novoselov KS, Katsnelson MI, Schedin F, Elias DC, Jaszczak JA, et al. Giant Intrinsic Carrier Mobilities in Graphene and Its Bilayer. Phys Rev Lett. 2008;100:016602.

[24] Das A, Pisana S, Chakraborty B, Piscanec S, Saha SK, Waghmare UV, et al. Monitoring dopants by Raman scattering in an electrochemically top-gated graphene transistor. Nature Nanotechnol. 2008;3:210.

[25] Kavan L, Rapta P, Dunsch L, Bronikowski MJ, Willis P, Smalley RE. Electrochemical Tuning of Electronic Structure of Single-Walled Carbon Nanotubes: In-situ Raman and Vis-NIR Study. J Phys Chem B. 2001;105:10764-10771.

[26] Blackburn JL, Barnes TM, Beard MC, Kim Y-H, Tenent RC, McDonald TJ, et al. Transparent Conductive Single-Walled Carbon Nanotube Networks with Precisely Tunable Ratios of Semiconducting and Metallic Nanotubes. ACS Nano. 2008;2:1266-1274.

[27] Geng H-Z, Kim KK, So KP, Lee YS, Chang Y, Lee YH. Effect of Acid Treatment on Carbon Nanotube-Based Flexible Transparent Conducting Films. J Am Chem Soc. 2007;129:7758-7759.

[28] Nirmalraj PN, Lyons PE, De S, Coleman JN, Boland JJ. Electrical Connectivity in Single-Walled Carbon Nanotube Networks. Nano Lett. 2009;9:3890-3895.

[29] Shim BS, Zhu J, Jan E, Critchley K, Kotov NA. Transparent Conductors from Layer-by-Layer Assembled SWNT Films: Importance of Mechanical Properties and a New Figure of Merit. ACS Nano. 2010;4:3725-3734.

[30] Wang Y, Di C-a, Liu Y, Kajiura H, Ye S, Cao L, et al. Optimizing Single-Walled Carbon Nanotube Films for Applications in Electroluminescent Devices. Adv Mater. 2008;20:4442-4449.

[31] Kim SM, Kim KK, Jo YW, Park MH, Chae SJ, Duong DL, et al. Role of Anions in the AuCl3-Doping of Carbon Nanotubes. ACS Nano. 2011;5:1236-1242.

[32] Murat A, Rungger I, Jin C, Sanvito S, Schwingenschlögl U. Origin of the p-Type Character of AuCl3 Functionalized Carbon Nanotubes. J Phys Chem C. 2014;118:3319-3323.

[33] Kim KK, Bae JJ, Park HK, Kim SM, Geng H-Z, Park KA, et al. Fermi Level Engineering of Single-Walled Carbon Nanotubes by AuCl3 Doping. J Am Chem Soc. 2008;130:12757-12761.

[34] Chen J, Dhall R, Hou B, Yang S, Wang B, Kang D, et al. Enhanced photoluminescence in air-suspended carbon nanotubes by oxygen doping. Appl Phys Lett. 2016;109:153109.

[35] Pal PP, Larionova T, Anoshkin IV, Jiang H, Nisula M, Goryunkov AA, et al. Dry Functionalization and Doping of Single-Walled Carbon Nanotubes by Ozone. J Phys Chem C. 2015;119:27821-27828.

[36] Miyauchi Y, Iwamura M, Mouri S, Kawazoe T, Ohtsu M, Matsuda K. Brightening of excitons in carbon nanotubes on dimensionality modification. Nature Photon. 2013;7:715.

[37] Jia Y, Cao A, Bai X, Li Z, Zhang L, Guo N, et al. Achieving High Efficiency Silicon-Carbon Nanotube Heterojunction Solar Cells by Acid Doping. Nano Lett. 2011;11:1901-1905.

[38] Kozawa D, Hiraoka K, Miyauchi Y, Mouri S, Matsuda K. Analysis of the Photovoltaic Properties of Single-Walled Carbon Nanotube/Silicon Heterojunction Solar Cells. Appl Phys Exp. 2012;5:042304.

[39] Wang F, Kozawa D, Miyauchi Y, Hiraoka K, Mouri S, Matsuda K. Enhancement Mechanism of the Photovoltaic Conversion Efficiency of Single-Walled Carbon Nanotube/Si Solar Cells by HNO 3 Doping. Appl Phys Exp. 2013;6:102301.

[40] Cui K, Anisimov AS, Chiba T, Fujii S, Kataura H, Nasibulin AG, et al. Air-stable high-efficiency solar cells with dry-transferred single-walled carbon nanotube films. J Mater Chem A. 2014;2:11311-11318.

[41] Cui T, Lv R, Huang Z-H, Chen S, Zhang Z, Gan X, et al. Enhanced efficiency of graphene/silicon heterojunction solar cells by molecular doping. J Mater Chem A. 2013;1:5736-5740.

[42] Ketolainen T, Havu V, Puska MJ. Conductivity of AuCl4-Functionalized Carbon Nanotube Networks. J Phys Chem C. 2017;121:4627-4634.

[43] Miao X, Tongay S, Petterson MK, Berke K, Rinzler AG, Appleton BR, et al. High Efficiency Graphene Solar Cells by Chemical Doping. Nano Lett. 2012;12:2745-2750.

[44] Jung Y, Li X, Rajan NK, Taylor AD, Reed MA. Record High Efficiency Single-Walled Carbon Nanotube/Silicon p–n Junction Solar Cells. Nano Lett. 2013;13:95-99.

[45] Davis VA, Parra-Vasquez ANG, Green MJ, Rai PK, Behabtu N, Prieto V, et al. True solutions of single-walled carbon nanotubes for assembly into macroscopic materials. Nature Nanotechnol. 2009;4:830.

[46] Goodrich A, Hacke P, Wang Q, Sopori B, Margolis R, James TL, et al. A wafer-based monocrystalline silicon photovoltaics road map: Utilizing known technology improvement opportunities for further reductions in manufacturing costs. Sol Energy Mater Sol Cells. 2013;114:110-135.

[47] Louwen A, van Sark W, Schropp R, Faaij A. A cost roadmap for silicon heterojunction solar cells. Sol Energy Mater Sol Cells. 2016;147:295-314.

[48] Bullock J, Hettick M, Geissbühler J, Ong AJ, Allen T, Sutter-Fella Carolin M, et al. Efficient silicon solar cells with dopant-free asymmetric heterocontacts. Nature Energy. 2016;1:15031.

[49] Jia Y, Li P, Gui X, Wei J, Wang K, Zhu H, et al. Encapsulated carbon nanotube-oxide-silicon solar cells with stable 10% efficiency. Appl Phys Lett. 2011;98:133115.

[50] Javey A, Tu R, Farmer DB, Guo J, Gordon RG, Dai H. High Performance n-Type Carbon Nanotube Field-Effect Transistors with Chemically Doped Contacts. Nano Lett. 2005;5:345-348.

[51] Rao AM, Eklund PC, Bandow S, Thess A, Smalley RE. Evidence for charge transfer in doped carbon nanotube bundles from Raman scattering. Nature. 1997;388:257-259.

[52] Zhou C, Kong J, Yenilmez E, Dai H. Modulated Chemical Doping of Individual Carbon Nanotubes. Science. 2000;290:1552-1555.

[53] Li X, Guard LM, Jiang J, Sakimoto K, Huang J-S, Wu J, et al. Controlled Doping of Carbon Nanotubes with Metallocenes for Application in Hybrid Carbon Nanotube/Si Solar Cells. Nano Lett. 2014;14:3388-3394.

[54] Sceats EL, Green JC. Noncovalent interactions between organometallic metallocene complexes and single-walled carbon nanotubes. J Chem Phys. 2006;125:154704.

[55] Li L-J, Khlobystov AN, Wiltshire JG, Briggs GAD, Nicholas RJ. Diameter-selective encapsulation of metallocenes in single-walled carbon nanotubes. Nature Mater. 2005;4:481-485.

[56] Lu J, Nagase S, Yu D, Ye H, Han R, Gao Z, et al. Amphoteric and Controllable Doping of Carbon Nanotubes by Encapsulation of Organic and Organometallic Molecules. Phys Rev Lett. 2004;93:116804.

[57] Li Z, Kunets VP, Saini V, Xu Y, Dervishi E, Salamo GJ, et al. Light-Harvesting Using High Density p-type Single Wall Carbon Nanotube/n-type Silicon Heterojunctions. ACS Nano. 2009;3:1407-1414.

[58] Eda G, Fanchini G, Chhowalla M. Large-area ultrathin films of reduced graphene oxide as a transparent and flexible electronic material. Nature Nanotechnol. 2008;3:270.

[59] Takenobu T, Takano T, Shiraishi M, Murakami Y, Ata M, Kataura H, et al. Stable and controlled amphoteric doping by encapsulation of organic molecules inside carbon nanotubes. Nature Mater. 2003;2:683.

[60] Fernández-Toribio JC, Íñiguez-Rábago A, Vilà J, González C, Ridruejo Á, Vilatela JJ. A Composite Fabrication Sensor Based on Electrochemical Doping of Carbon Nanotube Yarns. Adv Func Mater. 2016;26:7139-7147.

[61] Nonoguchi Y, Tani A, Ikeda T, Goto C, Tanifuji N, Uda RM, et al. Water-Processable, Air-Stable Organic Nanoparticle–Carbon Nanotube Nanocomposites Exhibiting n-Type Thermoelectric Properties. Small. 2017;13:1603420-n/a.

[62] Yu C, Murali A, Choi K, Ryu Y. Air-stable fabric thermoelectric modules made of N- and P-type carbon nanotubes. Energy Environ Sci. 2012;5:9481-9486.

[63] Sun D-m, Timmermans MY, Tian Y, Nasibulin AG, Kauppinen EI, Kishimoto S, et al. Flexible high-performance carbon nanotube integrated circuits. Nature Nanotechnol. 2011;6:156.

[64] Wadhwa P, Seol G, Petterson MK, Guo J, Rinzler AG. Electrolyte-Induced Inversion Layer Schottky Junction Solar Cells. Nano Lett. 2011;11:2419-2423.

[65] Wadhwa P, Liu B, McCarthy MA, Wu Z, Rinzler AG. Electronic Junction Control in a Nanotube-Semiconductor Schottky Junction Solar Cell. Nano Lett. 2010;10:5001-5005.

[66] Petterson MK, Lemaitre MG, Shen Y, Wadhwa P, Hou J, Vasilyeva SV, et al. On Field-Effect Photovoltaics: Gate Enhancement of the Power Conversion Efficiency in a Nanotube/Silicon-Nanowire Solar Cell. ACS Appl Mater Interf. 2015;7:21182-21187.

[67] Li X, Chen W, Zhang S, Wu Z, Wang P, Xu Z, et al. 18.5% efficient graphene/GaAs van der Waals heterostructure solar cell. Nano Energy. 2015;16:310-319.

[68] Wang P, Li X, Xu Z, Wu Z, Zhang S, Xu W, et al. Tunable graphene/indium phosphide heterostructure solar cells. Nano Energy. 2015;13:509-517.

[69] Regan W, Byrnes S, Gannett W, Ergen O, Vazquez-Mena O, Wang F, et al. Screening-Engineered Field-Effect Solar Cells. Nano Lett. 2012;12:4300-4304.

[70] Shih C-J, Pfattner R, Chiu Y-C, Liu N, Lei T, Kong D, et al. Partially-Screened Field Effect and Selective Carrier Injection at Organic Semiconductor/Graphene Heterointerface. Nano Lett. 2015;15:7587-7595.

[71] Kim K, Lee TH, Santos EJG, Jo PS, Salleo A, Nishi Y, et al. Structural and Electrical Investigation of C60–Graphene Vertical Heterostructures. ACS Nano. 2015;9:5922-5928.

[72] Hellstrom SL, Vosgueritchian M, Stoltenberg RM, Irfan I, Hammock M, Wang YB, et al. Strong and Stable Doping of Carbon Nanotubes and Graphene by MoOx for Transparent Electrodes. Nano Lett. 2012;12:3574-3580.

[73] Suriyasena Liyanage L, Xu X, Pitner G, Bao Z, Wong HSP. VLSI-Compatible Carbon Nanotube Doping Technique with Low Work-Function Metal Oxides. Nano Lett. 2014;14:1884-1890.

[74] Meyer J, Kidambi PR, Bayer BC, Weijtens C, Kuhn A, Centeno A, et al. Metal Oxide Induced Charge Transfer Doping and Band Alignment of Graphene Electrodes for Efficient Organic Light Emitting Diodes. Sc Rep. 2014;4:5380.

[75] Esconjauregui S, D'Arsié L, Guo Y, Yang J, Sugime H, Caneva S, et al. Efficient Transfer Doping of Carbon Nanotube Forests by MoO3. ACS Nano. 2015;9:10422-10430.

[76] Kahn A. Fermi level, work function and vacuum level. Mater Horiz. 2016;3:7-10.

[77] Greiner MT, Helander MG, Tang W-M, Wang Z-B, Qiu J, Lu Z-H. Universal energy-level alignment of molecules on metal oxides. Nature Mater. 2012;11:76-81.

[78] Yuan S, Rösner M, Schulz A, Wehling TO, Katsnelson MI. Electronic Structures and Optical Properties of Partially and Fully Fluorinated Graphene. Phys Rev Lett. 2015;114:047403.

[79] Wang B, Wang J, Zhu J. Fluorination of Graphene: A Spectroscopic and Microscopic Study. ACS Nano. 2014;8:1862-1870.

[80] Feng W, Long P, Feng Y, Li Y. Two-Dimensional Fluorinated Graphene: Synthesis, Structures, Properties and Applications. Adv Sci. 2016;3:1500413.

[81] Liu F, Jang M-H, Ha HD, Kim J-H, Cho Y-H, Seo TS. Facile Synthetic Method for Pristine Graphene Quantum Dots and Graphene Oxide Quantum Dots: Origin of Blue and Green Luminescence. Adv Mater. 2013;25:3657-3662.

[82] Loh KP, Bao Q, Eda G, Chhowalla M. Graphene oxide as a chemically tunable platform for optical applications. 2010;2:1015.

[83] Yavuz S, Kuru C, Choi D, Kargar A, Jin S, Bandaru PR. Graphene oxide as a p-dopant and an anti-reflection coating layer, in graphene/silicon solar cells. Nanoscale. 2016;8:6473-6478.

[84] Jiao K, Wang X, Wang Y, Chen Y. Graphene oxide as an effective interfacial layer for enhanced graphene/silicon solar cell performance. J Mater Chem C. 2014;2:7715-7721.

[85] Diao S, Zhang X, Shao Z, Ding K, Jie J, Zhang X. 12.35% efficient graphene quantum dots/silicon heterojunction solar cells using graphene transparent electrode. Nano Energy. 2017;31:359-366.

[86] Tung VC, Kim J, Huang J. Graphene Oxide:Single-Walled Carbon Nanotube-Based Interfacial Layer for All-Solution-Processed Multijunction Solar Cells in Both Regular and Inverted Geometries. Adv Energy Mater. 2012;2:299-303.

[87] Kim J, Tung VC, Huang J. Water Processable Graphene Oxide:Single Walled Carbon Nanotube Composite as Anode Modifier for Polymer Solar Cells. Adv Energy Mater. 2011;1:1052-1057.

[88] Kim J, Cote LJ, Kim F, Yuan W, Shull KR, Huang J. Graphene Oxide Sheets at Interfaces. J Am Chem Soc. 2010;132:8180-8186.

[89] Yu L, Tune D, Shearer C, Shapter J. Heterojunction Solar Cells Based on Silicon and Composite Films of Graphene Oxide and Carbon Nanotubes. ChemSusChem. 2015;8:2940-2947.

[90] Zhong M, Xu D, Yu X, Huang K, Liu X, Qu Y, et al. Interface coupling in graphene/fluorographene heterostructure for high-performance graphene/silicon solar cells. Nano Energy. 2016;28:12-18.

[91] JuL, Velasco Jr J, HuangE, KahnS, NosigliaC, Tsai H-Z, et al. Photoinduced doping in heterostructures of graphene and boron nitride. Nature Nanotechnol. 2014;9:348-352.

[92] Alexeev E, Moger J, Hendry E. Photo-induced doping and strain in exfoliated graphene. Appl Phys Lett. 2013;103:151907.

[93] Kim M, Safron NS, Huang C, Arnold MS, Gopalan P. Light-Driven Reversible Modulation of Doping in Graphene. Nano Lett. 2012;12:182-187.

[94] Wang X-J, Zou L, Li D, Zhang Q, Wang F, Zhang Z. Photo-Induced Doping in Graphene/Silicon Heterostructures. J Phys Chem C. 2015;119:1061-1066.

[95] Li X, Lin S, Lin X, Xu Z, Wang P, Zhang S, et al. Graphene/h-BN/GaAs sandwich diode as solar cell and photodetector. Opt Express. 2016;24:134-145.

[96] Wu J, Feng S, Wu Z, Lu Y, Lin S. Multi-type quantum dots photo-induced doping enhanced graphene/semiconductor solar cell. RSC Adv. 2017;7:33413-33418.

[97] Ho P-H, Li S-S, Liou Y-T, Wen C-Y, Chung Y-H, Chen C-W. Wavelength-Selective Dual p- and n-Type Carrier Transport of an Organic/Graphene/Inorganic Heterostructure. Adv Mater. 2015;27:282-287.

[98] Ho P-H, Lee W-C, Liou Y-T, Chiu Y-P, Shih Y-S, Chen C-C, et al. Sunlight-activated graphene-heterostructure transparent cathodes: enabling high-performance n-graphene/p-Si Schottky junction photovoltaics. Energy Environ Sci. 2015;8:2085-2092.

[99] Jiang K, Wang J, Li Q, Liu L, Liu C, Fan S. Superaligned Carbon Nanotube Arrays, Films, and Yarns: A Road to Applications. Adv Mater. 2011;23:1154-1161.

[100] Di J, Yong Z, Zheng X, Sun B, Li Q. Aligned Carbon Nanotubes for High-Efficiency Schottky Solar Cells. Small. 2013;9:1367-1372.

[101] Li X, Jung Y, Sakimoto K, Goh T-H, Reed MA, Taylor AD. Improved efficiency of smooth and aligned single walled carbon nanotube/silicon hybrid solar cells. Energy Environ Sci. 2013;6:879-887.

[102] Tune DD, Stolz BW, Pfohl M, Flavel BS. Dry shear aligning: a simple and versatile method to smooth and align the surfaces of carbon nanotube thin films. Nanoscale. 2016;8:3232-3236.

[103] Laiho P, Rafiee M, Liao Y, Hussain A, Ding E-X, Kauppinen EI. Wafer-Scale Thermophoretic Dry Deposition of Single-Walled Carbon Nanotube Thin Films. ACS Omega. 2018;3:1322-1328.

[104] Laiho P, Mustonen K, Ohno Y, Maruyama S, Kauppinen EI. Dry and Direct Deposition of Aerosol-Synthesized Single-Walled Carbon Nanotubes by Thermophoresis. ACS Appl Mater Interf. 2017;9:20738-20747.

[105] Cui K, Chiba T, Omiya S, Thurakitseree T, Zhao P, Fujii S, et al. Self-Assembled Microhoneycomb Network of Single-Walled Carbon Nanotubes for Solar Cells. J Phys Chem Lett. 2013;4:2571-2576.

[106] Fukaya N, Kim DY, Kishimoto S, Noda S, Ohno Y. One-Step Sub-10 μm Patterning of Carbon-Nanotube Thin Films for Transparent Conductor Applications. ACS Nano. 2014;8:3285-3293.

[107] Xu W, Wu S, Li X, Zou M, Yang L, Zhang Z, et al. High-Efficiency Large-Area Carbon Nanotube-Silicon Solar Cells. Adv Energy Mater. 2016;6:1600095.

[108] Shi E, Li H, Xu W, Wu S, Wei J, Fang Y, et al. Improvement of graphene–Si solar cells by embroidering graphene with a carbon nanotube spider-web. Nano Energy. 2015;17:216-223.

[109] Li X, Jung Y, Huang J-S, Goh T, Taylor AD. Device Area Scale-Up and Improvement of SWNT/Si Solar Cells Using Silver Nanowires. Advanced Energy Materials. 2014;4:1400186-n/a.

[110] Song J, Kam F-Y, Png R-Q, Seah W-L, Zhuo J-M, Lim G-K, et al. A general method for transferring graphene onto soft surfaces. Nature Nanotechnol. 2013;8:356.

[111] Ho P-H, Liou Y-T, Chuang C-H, Lin S-W, Tseng C-Y, Wang D-Y, et al. Self-Crack-Filled Graphene Films by Metallic Nanoparticles for High-Performance Graphene Heterojunction Solar Cells. Adv Mater. 2015;27:1724-1729.

[112] Xu D, He J, Yu X, Gao D, Ma L, Mu X, et al. Illumination-Induced Hole Doping for Performance Improvement of Graphene/n-Silicon Solar Cells with P3HT Interlayer. Adv Electron Mater. 2017;3:1600516-n/a.

[113] He H, Yu X, Wu Y, Mu X, Zhu H, Yuan S, et al. 13.7% Efficiency graphene–gallium arsenide Schottky junction solar cells with a P3HT hole transport layer. Nano Energy. 2015;16:91-98.

[114] Yu L, Batmunkh M, Grace T, Dadkhah M, Shearer C, Shapter J. Application of a hole transporting organic interlayer in graphene oxide/single walled carbon nanotube-silicon heterojunction solar cells. J Mater Chem A. 2017;5:8624-8634.

[115] Xu D, Yu X, Gao D, Mu X, Zhong M, Yuan S, et al. Room-temperature processed, air-stable and highly efficient graphene/silicon solar cells with an organic interlayer. J Mater Chem A. 2016;4:11284-11291.

[116] Li X, Zang X, Li X, Zhu M, Chen Q, Wang K, et al. Hybrid Heterojunction and Solid-State Photoelectrochemical Solar Cells. Adv Energy Mater. 2014;4:1400224-n/a.

[117] Li X, Jung Y, Huang J-S, Goh T, Taylor AD. Device Area Scale-Up and Improvement of SWNT/Si Solar Cells Using Silver Nanowires. Adv Energy Mater. 2014;4:n/a-n/a.

[118] Jia Y, Cao A, Kang F, Li P, Gui X, Zhang L, et al. Strong and reversible modulation of carbon nanotube-silicon heterojunction solar cells by an interfacial oxide layer. Phys Chem Chem Phys. 2012;14:8391-8396.

[119] Li X, Huang J-S, Nejati S, McMillon L, Huang S, Osuji CO, et al. Role of HF in Oxygen Removal from Carbon Nanotubes: Implications for High Performance Carbon Electronics. Nano Lett. 2014;14:6179-6184.

[120] Pintossi C, Pagliara S, Drera G, De Nicola F, Castrucci P, De Crescenzi M, et al. Steering the Efficiency of Carbon Nanotube–Silicon Photovoltaic Cells by Acid Vapor Exposure: A Real-Time Spectroscopic Tracking. ACS Appl Mater Interf. 2015;7:9436-9444.

[121] Watanabe K, Taniguchi T, Kanda H. Direct-bandgap properties and evidence for ultraviolet lasing of hexagonal boron nitride single crystal. Nature Mater. 2004;3:404.

[122] Xue J, Sanchez-Yamagishi J, Bulmash D, Jacquod P, Deshpande A, Watanabe K, et al. Scanning tunnelling microscopy and spectroscopy of ultra-flat graphene on hexagonal boron nitride. Nature Mater. 2011;10:282.

[123] Kubota Y, Watanabe K, Tsuda O, Taniguchi T. Deep Ultraviolet Light-Emitting Hexagonal Boron Nitride Synthesized at Atmospheric Pressure. Science. 2007;317:932-934.

[124] Hong X, Kim J, Shi S-F, Zhang Y, Jin C, Sun Y, et al. Ultrafast charge transfer in atomically thin MoS2/WS2 heterostructures. Nature Nanotechnol. 2014;9:682.

[125] Lee C-H, Lee G-H, van der Zande AM, Chen W, Li Y, Han M, et al. Atomically thin p–n junctions with van der Waals heterointerfaces. Nature Nanotechnol. 2014;9:676.

[126] Mak KF, Lee C, Hone J, Shan J, Heinz TF. Atomically Thin ${\mathrm{MoS}}_{2}$: A New Direct-Gap Semiconductor. Phys Rev Lett. 2010;105:136805.

[127] Meng J-H, Liu X, Zhang X-W, Zhang Y, Wang H-L, Yin Z-G, et al. Interface engineering for highly efficient graphene-on-silicon Schottky junction solar cells by introducing a hexagonal boron nitride interlayer. Nano Energy. 2016;28:44-50.

[128] Dean CR, Young AF, Meric I, Lee C, Wang L, Sorgenfrei S, et al. Boron nitride substrates for high-quality graphene electronics. Nature Nanotechnol. 2010;5:722.

[129] Liu Z, Ma L, Shi G, Zhou W, Gong Y, Lei S, et al. In-plane heterostructures of graphene and hexagonal boron nitride with controlled domain sizes. Nature Nanotechnol. 2013;8:119.

[130] Yankowitz M, Xue J, Cormode D, Sanchez-Yamagishi JD, Watanabe K, Taniguchi T, et al. Emergence of superlattice Dirac points in graphene on hexagonal boron nitride. Nature Phys. 2012;8:382.

[131] Tsuboi Y, Wang F, Kozawa D, Funahashi K, Mouri S, Miyauchi Y, et al. Enhanced photovoltaic performances of graphene/Si solar cells by insertion of a MoS2 thin film. Nanoscale. 2015;7:14476-14482.

[132] Jiao K, Duan C, Wu X, Chen J, Wang Y, Chen Y. The role of MoS2 as an interfacial layer in graphene/silicon solar cells. Phys Chem Chem Phys. 2015;17:8182-8186.

[133] Jariwala D, Davoyan AR, Wong J, Atwater HA. Van der Waals Materials for Atomically-Thin Photovoltaics: Promise and Outlook. ACS Photonics. 2017.

[134] Bernardi M, Palummo M, Grossman JC. Extraordinary Sunlight Absorption and One Nanometer Thick Photovoltaics Using Two-Dimensional Monolayer Materials. Nano Lett. 2013;13:3664-3670.

[135] Roy K, Padmanabhan M, Goswami S, Sai TP, Ramalingam G, Raghavan S, et al. Graphene–MoS2 hybrid structures for multifunctional photoresponsive memory devices. Nature Nanotechnol. 2013;8:826.

[136] Jariwala D, Sangwan VK, Wu C-C, Prabhumirashi PL, Geier ML, Marks TJ, et al. Gate-tunable carbon nanotube–MoS2 heterojunction p-n diode. Proc Nat Acad Sci. 2013;110:18076-18080.

[137] Kaltenbrunner M, White MS, Głowacki ED, Sekitani T, Someya T, Sariciftci NS, et al. Ultrathin and lightweight organic solar cells with high flexibility. Nature Commun. 2012;3:770.

[138] Jinno H, Fukuda K, Xu X, Park S, Suzuki Y, Koizumi M, et al. Stretchable and waterproof elastomer-coated organic photovoltaics for washable electronic textile applications. Nature Energy. 2017;2:780-785.

[139] Jean J, Wang A, Bulović V. In situ vapor-deposited parylene substrates for ultra-thin, lightweight organic solar cells. Org Electron. 2016;31:120-126.

[140] Ding K, Zhang X, Xia F, Wang R, Kuang Y, Duhm S, et al. Surface charge transfer doping induced inversion layer for high-performance graphene/silicon heterojunction solar cells. J Mater Chem A. 2017;5:285-291.

[141] Xu D, Yu X, Gao D, Li C, Zhong M, Zhu H, et al. Self-generation of a quasi p-n junction for high efficiency chemical-doping-free graphene/silicon solar cells using a transition metal oxide interlayer. J Mater Chem A. 2016;4:10558-10565.

[142] Tung RT. The physics and chemistry of the Schottky barrier height. Appl Phys Rev. 2014;1:011304.

[143] Jeon I, Cui K, Chiba T, Anisimov A, Nasibulin AG, Kauppinen EI, et al. Direct and Dry Deposited Single-Walled Carbon Nanotube Films Doped with MoOx as Electron-Blocking Transparent Electrodes for Flexible Organic Solar Cells. J Am Chem Soc. 2015;137:7982-7985.

[144] Jeon I, Chiba T, Delacou C, Guo Y, Kaskela A, Reynaud O, et al. Single-Walled Carbon Nanotube Film as Electrode in Indium-Free Planar Heterojunction Perovskite Solar Cells: Investigation of Electron-Blocking Layers and Dopants. Nano Lett. 2015;15:6665-6671.

[145] Wang X, Tian H, Mohammad MA, Li C, Wu C, Yang Y, et al. A spectrally tunable all-graphene-based flexible field-effect light-emitting device. Nature Commun. 2015;6:7767.

[146] Liu C-H, Chang Y-C, Norris TB, Zhong Z. Graphene photodetectors with ultra-broadband and high responsivity at room temperature. Nature Nanotechnol. 2014;9:273.

[147] Zhao J, Wang A, Green MA, Ferrazza F. 19.8% efficient "honeycomb" textured multicrystalline and 24.4% monocrystalline silicon solar cells. Appl Phys Lett. 1998;73:1991-1993.

[148] Ye X, Zou S, Chen K, Li J, Huang J, Cao F, et al. 18.45%-Efficient Multi-Crystalline Silicon Solar Cells with Novel Nanoscale Pseudo-Pyramid Texture. Adv Func Mater. 2014;24:6708-6716.

[149] Zhong S, Huang Z, Lin X, Zeng Y, Ma Y, Shen W. High-Efficiency Nanostructured Silicon Solar Cells on a Large Scale Realized Through the Suppression of Recombination Channels. Adv Mater. 2015;27:555-561.

[150] Ali M, Zhou F, Chen K, Kotzur C, Xiao C, Bourgeois L, et al. Nanostructured photoelectrochemical solar cell for nitrogen reduction using plasmon-enhanced black silicon. Nature Commun. 2016;7:11335.

[151] Oh J, Yuan H-C, Branz HM. An 18.2%-efficient black-silicon solar cell achieved through control of carrier recombination in nanostructures. Nature Nanotechnol. 2012;7:743.

[152] Savin H, Repo P, von Gastrow G, Ortega P, Calle E, Garín M, et al. Black silicon solar cells with interdigitated back-contacts achieve 22.1% efficiency. Nature Nanotechnol. 2015;10:624.

[153] Tian B, Zheng X, Kempa TJ, Fang Y, Yu N, Yu G, et al. Coaxial silicon nanowires as solar cells and nanoelectronic power sources. Nature. 2007;449:885.

[154] Shi E, Zhang L, Li Z, Li P, Shang Y, Jia Y, et al. TiO2-Coated Carbon Nanotube-Silicon Solar Cells with Efficiency of 15%. Sci Rep. 2012;2:884.

[155] Shi E, Li H, Yang L, Zhang L, Li Z, Li P, et al. Colloidal Antireflection Coating Improves Graphene–Silicon Solar Cells. Nano Lett. 2013;13:1776-1781.

[156] Jiang K, Li Q, Fan S. Nanotechnology: Spinning continuous carbon nanotube yarns. Nature. 2002;419:801-801.

[157] Li R, Di J, Yong Z, Sun B, Li Q. Polymethylmethacrylate coating on aligned carbon nanotube-silicon solar cells for performance improvement. J Mater Chem A. 2014;2:4140-4143.

[158] Fan Q, Zhang Q, Zhou W, Xia X, Yang F, Zhang N, et al. Novel approach to enhance efficiency of hybrid silicon-based solar cells via synergistic effects of polymer and carbon nanotube composite film. Nano Energy. 2017;33:436-444.

[159] He H, Yu X, Wu Y, Mu X, Zhu H, Yuan S, et al. 13.7% Efficiency graphene–gallium arsenide Schottky junction solar cells with a P3HT hole transport layer. Nano Energy. 2015;16:91-98.

[160] Ueno K, Oshikiri T, Sun Q, Shi X, Misawa H. Solid-State Plasmonic Solar Cells. Chem Rev. 2018;118:2955–2993.

[161] Ferry VE, Verschuuren MA, Li HBT, Verhagen E, Walters RJ, Schropp REI, et al. Light trapping in ultrathin plasmonic solar cells. Opt Express. 2010;18:A237-A245.

[162] Tan H, Santbergen R, Smets AHM, Zeman M. Plasmonic Light Trapping in Thin-film Silicon Solar Cells with Improved Self-Assembled Silver Nanoparticles. Nano Lett. 2012;12:4070-4076.

[163] Spinelli P, Polman A. Prospects of near-field plasmonic absorption enhancement in semiconductor materials using embedded Ag nanoparticles. Opt Express. 2012;20:A641-A654.

[164] Pala RA, White J, Barnard E, Liu J, Brongersma ML. Design of Plasmonic Thin-Film Solar Cells with Broadband Absorption Enhancements. Adv Mater. 2009;21:3504-3509.

[165] Atwater HA, Polman A. Plasmonics for improved photovoltaic devices. Nature Mater. 2010;9:205.

[166] Cushing SK, Wu N. Progress and Perspectives of Plasmon-Enhanced Solar Energy Conversion. J Phys Chem Lett. 2016;7:666-675.

[167] Ding IK, Zhu J, Cai W, Moon S-J, Cai N, Wang P, et al. Plasmonic Dye-Sensitized Solar Cells. Adv Energy Mater. 2011;1:52-57.

[168] Sefunc MA, Okyay AK, Demir HV. Plasmonic backcontact grating for P3HT:PCBM organic solar cells enabling strong optical absorption increased in all polarizations. Opt Express. 2011;19:14200-14209.

[169] Zhou D, Liu D, Jin J, Chen X, Xu W, Yin Z, et al. Semiconductor plasmon-sensitized broadband upconversion and its enhancement effect on the power conversion efficiency of perovskite solar cells. J Mater Chem A. 2017;5:16559-16567.

[170] Cheng Y, Chen C, Chen X, Jin J, Li H, Song H, et al. Considerably enhanced perovskite solar cells via the introduction of metallic nanostructures. J Mater Chem A. 2017;5:6515-6521.

[171] Fan R, Wang L, Chen Y, Zheng G, Li L, Li Z, et al. Tailored Au@TiO2 nanostructures for the plasmonic effect in planar perovskite solar cells. J Mater Chem A. 2017;5:12034-12042.

[172] Zhang W, Saliba M, Stranks SD, Sun Y, Shi X, Wiesner U, et al. Enhancement of Perovskite-Based Solar Cells Employing Core–Shell Metal Nanoparticles. Nano Lett. 2013;13:4505-4510.

[173] Zhou C, Wang S, Sun J, Wei N, Yang L, Zhang Z, et al. Plasmonic enhancement of photocurrent in carbon nanotube by Au nanoparticles. Appl Phys Lett. 2013;102:103102.

[174] Li Y, Kodama S, Kaneko T, Hatakeyama R. Performance enhancement of solar cells based on single-walled carbon nanotubes by Au nanoparticles. Appl Phys Lett. 2012;101:083901.

[175] Huang K, Yan Y, Yu X, Zhang H, Yang D. Graphene coupled with Pt cubic nanoparticles for high performance, air-stable graphene-silicon solar cells. Nano Energy. 2017;32:225-231.

[176] Fang Z, Wang Y, Liu Z, Schlather A, Ajayan PM, Koppens FHL, et al. Plasmon-Induced Doping of Graphene. ACS Nano. 2012;6:10222-10228.

[177] Brongersma ML, Halas NJ, Nordlander P. Plasmon-induced hot carrier science and technology. Nature Nanotechnol. 2015;10:25.

[178] Luo L-B, Xie C, Wang X-H, Yu Y-Q, Wu C-Y, Hu H, et al. Surface plasmon resonance enhanced highly efficient planar silicon solar cell. Nano Energy. 2014;9:112-120.

[179] Grigorenko AN, Polini M, Novoselov KS. Graphene plasmonics. Nature Photon. 2012;6:749.

[180] Kramberger C, Hambach R, Giorgetti C, Rümmeli MH, Knupfer M, Fink J, et al. Linear Plasmon Dispersion in Single-Wall Carbon Nanotubes and the Collective Excitation Spectrum of Graphene. Phys Rev Lett. 2008;100:196803.

[181] Igarashi T, Kawai H, Yanagi K, Cuong NT, Okada S, Pichler T. Tuning Localized Transverse Surface Plasmon Resonance in Electricity-Selected Single-Wall Carbon Nanotubes by Electrochemical Doping. Phys Rev Lett. 2015;114:176807.

[182] Chiu K-C, Falk AL, Ho P-H, Farmer DB, Tulevski G, Lee Y-H, et al. Strong and Broadly Tunable Plasmon Resonances in Thick Films of Aligned Carbon Nanotubes. Nano Lett. 2017;17:5641-5645.

[183] Rodrigo D, Limaj O, Janner D, Etezadi D, García de Abajo FJ, Pruneri V, et al. Mid-infrared plasmonic biosensing with graphene. Science. 2015;349:165-168.

[184] Shu X-q, Zhang H, Cheng X-l, Miyamoto Y. Tunable plasmons in few-layer nitrogen-doped graphene nanostructures: A time-dependent density functional theory study. Physical Review B. 2016;93:195424.

[185] Wang Z, Li T, Almdal K, Asger Mortensen N, Xiao S, Ndoni S. Experimental demonstration of graphene plasmons working close to the near-infrared window. Opt Lett. 2016;41:5345-5348.

[186] Morimoto T, Joung S-K, Saito T, Futaba DN, Hata K, Okazaki T. Length-Dependent Plasmon Resonance in Single-Walled Carbon Nanotubes. ACS Nano. 2014;8:9897-9904.

[187] Yu L, Shearer C, Shapter J. Recent Development of Carbon Nanotube Transparent Conductive Films. Chem Rev. 2016;116:13413-13453.

[188] Hofstetter J, del Cañizo C, Wagner H, Castellanos S, Buonassisi T. Material requirements for the adoption of unconventional silicon crystal and wafer growth techniques for high-efficiency solar cells. Prog Photovolt Res Appl. 2016;24:122-132.

[189] Yang X, Ji L, Zou X, Lim T, Zhao J, Yu ET, et al. Toward Cost-Effective Manufacturing of Silicon Solar Cells: Electrodeposition of High-Quality Si Films in a CaCl2-based Molten Salt. Angew Chem Int Edn. 2017;129:15274-15278.

[190] Rogers JA, Lagally MG, Nuzzo RG. Synthesis, assembly and applications of semiconductor nanomembranes. Nature. 2011;477:45.

[191] Ruan K, Ding K, Wang Y, Diao S, Shao Z, Zhang X, et al. Flexible graphene/silicon heterojunction solar cells. J Mater Chem A. 2015;3:14370-14377.

[192] Jiao T, Wei D, Liu J, Sun W, Jia S, Zhang W, et al. Flexible solar cells based on graphene-ultrathin silicon Schottky junction. RSC Adv. 2015;5:73202-73206.

[193] Ahn J, Chou H, Banerjee SK. Graphene-Al2O3-silicon heterojunction solar cells on flexible silicon substrates. J Appl Phys. 2017;121:163105.

[194] Li X, Mariano M, McMillon-Brown L, Huang J-S, Sfeir MY, Reed MA, et al. Charge Transfer from Carbon Nanotubes to Silicon in Flexible Carbon Nanotube/Silicon Solar Cells. Small. 2017;13:1702387-n/a.

[195] Ahn N, Jeon I, Yoon J, Kauppinen EI, Matsuo Y, Maruyama S, et al. Carbon-sandwiched perovskite solar cell. J Mater Chem A. 2018;6:1382-1389.

[196] Jeon I, Yoon J, Ahn N, Atwa M, Delacou C, Anisimov A, et al. Carbon Nanotubes versus Graphene as Flexible Transparent Electrodes in Inverted Perovskite Solar Cells. J Phys Chem Lett. 2017;8:5395-5401.

[197] Yoon J, Sung H, Lee G, Cho W, Ahn N, Jung HS, et al. Superflexible, high-efficiency perovskite solar cells utilizing graphene electrodes: towards future foldable power sources. Energy Environ Sci. 2017;10:337-345.

[198] Song Y, Chang S, Gradecak S, Kong J. Visibly-Transparent Organic Solar Cells on Flexible Substrates with All-Graphene Electrodes. Adv Energy Mater. 2016;6:1600847.